

Supplementary Materials for

Brain metabolism modulates neuronal excitability in a mouse model of pyruvate dehydrogenase deficiency

Vikram Jakkamsetti, Isaac Marin-Valencia, Qian Ma, Levi B. Good, Tyler Terrill, Karthik Rajasekaran, Kumar Pichumani, Chalermchai Khemtong, M. Ali Hooshyar, Chandrasekhar Sundarajan, Mulchand S. Patel, Robert M. Bachoo, Craig R. Malloy, Juan M. Pascual*

*Corresponding author. Email: juan.pascual@utsouthwestern.edu

Published 20 February 2019, *Sci. Transl. Med.* **11**, eaan0457 (2019)

DOI: 10.1126/scitranslmed.aan0457

The PDF file includes:

Methods

Fig. S1. Glucose metabolism schema and survival curves of patients and mice with PDHD.

Fig. S2. Expression of PDH in the mouse somatosensory cortex.

Fig. S3. Phenotype of PDHD mice.

Fig. S4. Glucose metabolism in PDHD mice.

Fig. S5. EEG in patients with PDHD.

Fig. S6. Patient with PDHD EEG (patient I).

Fig. S7. EEG oscillation epochs in patients with PDHD.

Fig. S8. Cortical layering, evoked LFP, and baseline EEG in PDHD mice.

Fig. S9. Sorting of multiunit action potentials into single units and separation into broad- and fast-spiking neuronal origin.

Fig. S10. In vivo RS neuron discharge relative to fast-spiking activity.

Fig. S11. Brain slice intracellular recordings illustrating cell discrimination, rheobase, and firing.

Fig. S12. Neuronal input resistance under energetic substrate deprivation.

Fig. S13. EEG gamma power in relation to epileptiform events in PDHD.

Fig. S14. Gamma power in relation to epileptiform events in additional patients with PDHD.

Fig. S15. Acetate modulation of evoked LFPs in vivo.

Fig. S16. Acetate modulation of spontaneous excitatory postsynaptic currents.

Fig. S17. Modulation of input resistance and firing with acetate.

Fig. S18. Acetate modulation of EEG epileptiform events in awake mice.

Fig. S19. EEG epileptiform events in awake mice with vehicle injections.

Fig. S20. Representation of glucose oxidation and excitability coupling in relation to PDH activity.

Table S1. Plasma metabolite concentration.

Table S2. Isotopomer analysis of [U-¹³C]glucose NMR spectra from cerebral cortex NMR spectra.

Table S3. Isotopomers derived from [1,2-¹³C]acetate and [1,6-¹³C]glucose in cerebral cortex NMR spectra.

Table S4. Metabolic model analysis of glutamate and glutamine C4 multiplets from [1,6-¹³C]glucose and [1,2-¹³C]acetate cerebral cortex spectra.

Table S5. Modified Racine's scale.

Table S6. Key clinical features of patients with PDHD.

Legend for table S7

Legend for movie S1

References (57–75)

Other Supplementary Material for this manuscript includes the following:

(available at www.sciencetranslationalmedicine.org/cgi/content/full/11/480/eaan0457/DC1)

Table S7. Raw data (provided as a separate Excel file).

Movie S1 (.mp4 format). PDHD mouse video-EEG recording of epileptiform events.

SUPPLEMENTARY METHODS

Generation of brain-specific pyruvate dehydrogenase-deficient (PDHD) mice

Brain-specific C57BL6 *Pdha1*-deficient mice were generated by breeding *Pdha1*^{flox/flox} females (8) with *hGFAP-Cre* males. Genotyping of *Pdha1* (sense primer 5'-AGCAGCCAGCACGGACTACT-3' and antisense primer 5'-GCAGCCAAACAGATTACACC-3') and the *Cre* transgene (using 5'-ATTTGCCTGCATTACCGGTC-3' and 5'-ATCAACGTTTTCTTTTCGG-3') was carried out by PCR at two weeks of age. Males were used for functional studies due to their severe phenotype. All animal studies were approved by the Institutional Animal Care and Use Committee (IACUC) of UT Southwestern Medical Center.

Pyruvate dehydrogenase (PDH) activity

Mouse brains were harvested from P21-25 control and PDHD males (n= 8) after decapitation and snap frozen in liquid nitrogen. Total and active PDH complex activities were assayed as reported (57, 58) with modifications. To determine total PDH complex activity, pulverized tissue was homogenized at 4°C using a homogenizer powered by an overhead electric motor (20 strokes at 200 rpm) in 10 vol. (w/v) of extraction buffer containing 30 mM HEPES KOH (pH 7.5), 250 mM sucrose, 1 mM EGTA, 1 mM EDTA, 5 mM DTT (dithiothreitol), 1% fatty acid free BSA and EDTA-free complete protease inhibitor cocktail (catalog number 05892791001, Roche). For active PDH complex determination, 2 mM DCA (dichloroacetate) and 50mM KF (potassium fluoride) were added to the extraction buffer to preserve the in vivo phosphorylated state. The brain homogenate was centrifuged at 2000 g for 3 min and the supernatant was subsequently centrifuged at 12000 g for 10 min. The pellet was resuspended in 1 ml of 30 mM HEPES KOH (pH 7.5) and 250 mM sucrose and centrifuged at 12000 g for 10 min. The last step was repeated twice to obtain a mitochondria-enriched fraction, which was then suspended in 0.2 ml of

resuspension buffer containing 30 mM HEPES KOH (pH 7.5), 0.2 mM EDTA, 1% BSA, 5 mM DTT and EDTA-free complete protease inhibitor cocktail (diluted 1:50). The protein concentrations of mitochondria samples was determined with a BCA protein assay kit (catalog number 23225, Thermo Scientific). Both total and active mitochondrial PDH complex activities were measured using a pyruvate dehydrogenase complex activity microplate assay kit (catalog number ab109902, Abcam) as instructed by the manufacturer.

Active PDH complex activity was measured directly. Total PDH complex activity was measured after full activation by dephosphorylation with lambda protein phosphatase (59). Briefly, 150 μ g of crude mitochondria were incubated with 15 μ l of 10 \times phosphatase buffer, 5 μ l of 10 \times MnCl₂, 5.25 μ l of 125 mM of dichloroacetic acid, 1.5 μ l of lambda protein phosphatase (catalog number P07531, New England Biolabs) in a 150 μ l volume (adjusted with resuspension buffer) for 30min at 30°C.

¹³C NMR sample preparation

Mice were fasted for 5 hr prior to injection and remained awake during all experiments. For [U-¹³C]glucose studies, 7 control and 5 PDHD 21-22 day old mice were used. [U-¹³C]glucose (Cambridge Isotope Laboratories) was injected intraperitoneally at 2 mg/g of body weight from a 66 mg/ml saline dilution. Cortex and blood samples were collected 1 hr after injection. Mice were decapitated and the cortex dissected in less than 20 s, frozen in liquid nitrogen and stored at -80°C. Blood was simultaneously collected from the cervical stump and glucose concentration measured using a clinical glucometer. The metabolism of [1,6-¹³C]glucose (1-¹³C, 99% enriched; 6-¹³C, 97% enriched) and [1,2-¹³C₂]-acetate (1-¹³C, 99% enriched; 2-¹³C, 99% enriched, Cambridge Isotope Laboratories) was studied in 10 21-22 day old control and 10 PDHD mice. 2 mg/g of both ¹³C substrates were administered from a 66 mg/ml saline dilution at pH 7.4. Cortex

and blood samples were collected 1 hr after the injection and blood glucose concentration was determined as above. Cortex samples were processed via perchloric acid extraction (13). Once lyophilized, 160 μ l of deuterium oxide (99.96%, Cambridge Isotope Laboratories) and 20 μ l of 2,2-dimethyl-2-silapentane-3,3,4,4,5,5-*d*₆-5-sulfonate sodium salt (DSS-*d*₆, Chenomx) were added to each sample and the pH adjusted to 7.0 with sodium deuterioxide (99.5%, Cambridge Isotope Laboratories). Samples were then centrifuged at 18,400 *g* for 1 min and the supernatant removed and placed into 3-mm NMR tubes for NMR analysis.

Mass spectrometry

Absolute metabolite concentrations of amino acids, TCA cycle intermediates and coenzymes A in forebrain, and of lactate, β -hydroxybutyrate and acetoacetate in plasma were determined at the Mouse Metabolic Phenotypic Center at Case Western Reserve University (60). The ¹³C enrichment of plasma glucose was measured as described (61).

Mathematical model

The estimation of glucose and acetate metabolic compartmentation in cortex utilized a mathematical model (18). The model incorporated the isotopomer analysis of glutamate and glutamine C4. Based on the notion that neurons use glucose as an energy substrate and that oxidation of acetate and glucose occurs in astrocytes, the model estimated the ¹³C distribution of glutamate and glutamine originated in each of these two putative cell compartments after the administration of [1,2-¹³C]acetate and [1,6-¹³C]glucose. To this effect, the model defined specific variables according to the relative area of multiplets of each isotopomer derived from [1,2-¹³C]acetate and [1,6-¹³C]glucose in astrocytes and from [1,6-¹³C]glucose in neurons, weighing the contribution of each cell compartment to the total glutamate and glutamine spectrum, and

estimated the acetate: glucose oxidative ratio by dividing the values derived from [1,2-¹³C]acetate by those from [1,6-¹³C]glucose ((18), Table S4).

Western blot

Following a 5 hr fast, 23-26 day old mice (4 males in each group,) were decapitated and their cortices manually dissected quickly, immersed in liquid nitrogen and kept at -80°C. Cortex proteins were extracted using radioimmunoprecipitation assay (RIPA) buffer containing protease inhibitor cocktail (Roche) and homogenized under ice with an ultrasonic processor. The insoluble material was removed from the protein extracts by centrifugation at 14,000 rpm for 15 min at 4°C. Protein content was quantified by BCA assay (Bio-Rad). Approximately 60 µg of total protein per sample was separated in 4–20% gradient SDS-PAGE gels (Bio-Rad) and transferred to nitrocellulose membranes. The membranes were blocked with BSA (5%) in TRIS-buffered saline, 0.1% Tween 20 (TBST) for 1 h and then incubated overnight with primary antibody to PDHA1 (rabbit monoclonal, 1:1000, Abcam). They were then washed three times with TBST, followed by incubation of rabbit HRP-conjugated secondary antibody (1:10,000, Santa Cruz Biotechnology) for 1 hr. Membranes were then washed three times and treated with Pierce ECL Western Blotting Substrate (Thermo Scientific) prior to chemiluminescent visualization (Chemidoc system, Bio-Rad). Blots were stripped using Restore fluorescence western blot stripping buffer (Thermo Scientific) and reprobbed with β-actin (1:5000, Sigma, St. Louis, MO) as control. PDHA1 levels were determined by band densitometry and normalized to β-actin using ImageJ (62).

Histology

Mice were anesthetized with ketamine and xylazine as above and perfused transcardially with cold 4% paraformaldehyde (PFA) in 0.1 M phosphate buffer (pH 7.4). Brains were dissected and

additionally fixed overnight in 4% PFA at 4°C. They were then sequentially processed in 15 % (1 day) and 30 % (1 day) sucrose in 0.1M PBS at 4°C, embedded in optimal cutting temperature compound (O.C.T.) and sliced into 12 µm sections. Sections were collected on Superfrost Plus glass slides (Thermo Scientific). The sections were stained with 0.25% cresyl violet in sodium acetate to reveal cell nuclei. All slides were digitized using a Nanozoomer 2.0 HT whole slide scanner (Hamamatsu Photonics) and visualized with NDP View software (Hamamatsu Photonics).

Prior to immunofluorescence staining, fixed brains were blocked in 3% agarose. Forebrains were cut in 40 µm coronal sections on a vibratome (VT1200s, Leica). Sections were cryoprotected and stored at -20°C. For double immunostaining, free floating forebrain sections were first washed with 0.1 M PBS and then incubated in a blocking buffer with 5% normal goat serum and 0.3% Triton X-100 in 0.1 M PBS for 2 h at 4°C. Sections were then incubated in a mixture of rabbit anti-PDHA1 (Rabbit anti-PDH E1-alpha subunit ab110474, 1:500, Abcam) and mouse anti-NeuN (mouse anti-NeuN, mab377, 1:1000, MilliporeSigma) overnight at 4°C. After washing for 10 min with 0.1 M PBS 3 times, sections were incubated with mixed Alexa flour 488-conjugated goat anti-rabbit IgG and Alexa flour 594-conjugated goat anti-mouse IgG (A-11008 and A-11032, both 1:500, Thermo Scientific) for 2h at room temperature. After rinsing in 0.1 M PBS 3 times (10 min each), sections were counterstained with 4',6-diamidino-2-phenylindole (DAPI, 1:5000, Thermo Scientific). For glial fibrillary acidic protein (GFAP) staining, sections were first stained with anti-PDHA1 (Alexa Fluor 488, Thermo Scientific) and then rabbit anti-GFAP (catalog number Z0334, 1:1000, Agilent) following the same procedure. All immunofluorescently stained sections were scanned with a Laser Scanning Microscope (LSM 510, Carl Zeiss) and analyzed using Image J.

Immunohistochemical staining of MAP2 was performed using an Avidin Biotin Complex (ABC) method. Briefly, free-floating sections were permeabilized with 0.3 Triton X-100 in 0.1M PBS and washed thrice. They were then incubated in 1% hydrogen peroxide in 0.1M PBS for 30 min, washed thrice and blocked with 5 normal goat serum at room temperature for 2h. Sections were then incubated overnight at 4°C with rabbit anti-MAP2 primary antibody (Abcam ab32454, 1:500). They were then washed and incubated with secondary biotinylated goat anti-rabbit antibody (catalog number BA-1000, 1:500, Vector) for 2h at room temperature. Samples were washed with PBS three times and then incubated in Avidin Biotinylated Enzyme Complex (ABC) solution (Vector PK-6100) for 2h. After washing with 0.1M PBS, sections were added to a well containing NovaRED (Vector SK-4800) for 3 min, washed again and plated to slides. The slides were then sequentially placed in 70%, 95% and 100 % ethanol baths, cover-slipped with Permount (SP15-500, Thermo Scientific) and imaged whole-slide in a Hamamatsu Nanozoomer 2.0 HT.

Somatosensory cortical thickness was determined in DAPI-stained coronal brain sections. Serial 40 µm sections spanned from 1.32 mm to -2.75 mm relative to bregma (n= 3 mice) at an interval of 240 µm. They were stained and then imaged with the Nanozoomer. Cortical thickness was measured at identical antero-posterior positions and at the same medio-lateral level in 3 sections of each mouse using NDP View software (Hamamatsu).

¹³C NMR spectroscopy

Proton and carbon NMR spectra were generated as described (13). Briefly, proton decoupled ¹³C spectra were acquired on a 600 MHz Oxford magnet and Agilent Drive console using a 3 mm broadband probe (Agilent). Proton decoupling was performed using a Waltz-16 sequence.

Parameters included a 45° flip angle per transient, a relaxation delay of 1.5 s, an acquisition time of 1.5 s, and a spectral width of 34.5 kHz. Samples were spun at 20 Hz and 25°C. A heteronuclear 2H lock was used to compensate for magnet drift during data acquisition. To achieve adequate signal-to-noise in brain spectra the number of scans acquired were typically 16,000 to 22,000. Proton spectra were similarly acquired. Parameters included a 45° flip angle per transient, a relaxation delay of 1 s, an acquisition time of 2 s and a spectral width of 20 kHz. Samples were spun and the temperature maintained as for the ¹³C spectra. A heteronuclear 2H lock was also used. The number of scans per sample was 120. NMR spectral analyses were performed using ACD/Spec Manager 11.0 software (Advanced Chemistry Development) as published (13). Chenomx NMR Suite (Chenomx) was used to quantify metabolite concentration in proton NMR spectrum. The enrichment of ¹³C acetyl-CoA was calculated from glutamate C4 using a published non-steady state analysis (63).

Measurement of plasma acetate

Acetate was measured using a modified version of a commercial protocol (Acetate Colorimetric Assay Kit, K658-100, Biovision). In brief, after a 5 hr fast, mice were decapitated and approximately 200 µL of blood were collected in pre-cooled EDTA tubes. The tubes were centrifuged at 6,000 g for 10 min at 4 °C. The plasma was recovered, placed in centrifugal filters (Millipore) and centrifuged at 14,000 g for 40 min at 4°C. The acetate standard was diluted to 1 mM and 0, 0.5, 1, 1.5, 2, 2.5, 3, 3.5 µl were added in triplicate into series of wells in a 380 well plate. The final volume was adjusted to 12.5 µl with water. 1 µl of each plasma sample was added in triplicate and the final volume was adjusted to 12.5 µl with water. The Reaction Mix included 10.5 µl of Acetate Assay Buffer, 0.5 µl Acetate Enzyme Mix, 0.5 µl ATP, 0.5 µl Acetate Substrate Mix, and 0.5 µl Probe. 12.5 µl of the reaction mix were added to each standard

and sample. The Background Control Mix was prepared using the same formulation as the Reaction Mix without Acetate Enzyme Mix, and 12.5 μ l were added in one series of triplicate to sample background control wells. The reaction was incubated at room temperature for 40 min, and the absorbance was measured at OD_{450nm}. The acetate concentration was calculated following the manufacturer's protocol.

Lifespan of patients with PDHD

The English literature containing the keyword "pyruvate dehydrogenase deficiency" was reviewed in PubMed including publications from 1970 to March 2015, in addition to references included in articles found through the search term. The age at death (in months) was included for all patients who were followed to death in the publications. Kaplan-Meier estimator analysis was conducted using Prism 6.0 (GraphPad).

In vivo intracortical mouse electrophysiological recording

Surgery and recording: Male PDHD and control mice aged P21-P25 were used for in vivo recording. To facilitate a uniform metabolic state in anesthetized, fasting mice, experiments (surgery and recording) were completed within 3 hr after anesthesia induction. In most cases only one recording site per mouse was accessed. For any subsequent recording, a site more than 250 μ m away was used. After induction of anesthesia with i.p injection of ketamine (100 mg/kg), xylazine (10 mg/kg) and acepromazine (2 mg/kg), a craniotomy over the barrel cortex was performed. Anesthesia was maintained with the same dose of supplemental ketamine at 45 min – 1 hr intervals (based on toe-pinch withdrawal-reflexes) and with the same dose of supplemental xylazine for recordings lasting more than 2 hr after induction. Core body temperature was measured with a rectal probe and maintained at 37°C with a temperature controller (TC-1000,

CWE). The exposed dura was kept moist with saline throughout experiments. Care was taken to avoid surface blood vessels during microelectrode insertion. Electrodes were designed as a vertical array of four electrode sites, with a circular recording area of $177 \mu\text{m}^2$ for recording spontaneous local field potentials (NeuroNexus). Histological studies established that layer 2/3 is located $100 - 350 \mu\text{m}$ deep in control and $50 - 250 \mu\text{m}$ deep in PDHD mice. Electrophysiological activity was acquired at a sampling rate of 50 kHz, amplified and filtered (bandpass, 400 – 20,000 Hz) with a MultiClamp 700B amplifier (Molecular Devices).

Intracortical stimulation: We positioned layer 2/3 recording electrodes at the depth where maximum evoked LFP response was obtained after stimulating $300 \mu\text{m}$ deeper. The electrodes had a surface area of $703 \mu\text{m}^2$ (NeuroNexus). An activated iridium oxide electrode (impedance $0.04 - 0.07 \text{ M}\Omega$) was used for stimulation. Electrode position in the barrel cortex was confirmed by the recording of action potentials after passive stimulation of contralateral whiskers. For the characterization of input-output curves, each stimulus current (from $0 - 40 \mu\text{A}$ administered in $5 \mu\text{A}$ steps) was applied five times (15 s apart). For the determination of temporal response properties, a single sub-maximal current stimulus capable of eliciting a robust response was repetitively applied in trains of stimuli 30 s apart. Each train included 6 stimuli. Interstimulus intervals were $5, 1, 0.5, 0.1, 0.05,$ and 0.025 s .

Whiskerpad-evoked action potentials: Two stimulating needle electrodes insulated to the point of entry into the skin were inserted between whisker rows A&B (parallel to the long axis of the whisker rows) and C&D (along the entire length of the whisker rows). Unipolar biphasic current pulses of 2 ms and 1.9 mA were administered 3 s apart for 200 trials. Electrophysiological data acquisition included 1 s prior to 1 s following whisker-pad stimulation. Tungsten microelectrodes ($3 \mu\text{m}$ insulation, 0.356 mm shaft, $2 \text{ M}\Omega$, $1\text{-}2 \mu\text{m}$ tip, World Precision Instruments) were inserted orthogonally to the barrel cortex surface and advanced to a priori

histologically located layer 4/5. Thus, recording was conducted at a depth of 450 – 500 μm in control and 350 – 400 μm in PDHD. The location of the recording tip was confirmed by tissue electrolytic burn at the conclusion of recording (fig. S8A).

Acetate modulation: A 1 ml syringe connected to tubing primed with acetate solution was attached to an intraperitoneally inserted winged infusion set (27 g \times 1/2 inch, 20 cm tubing length) prior to recording electrode placement. Microelectrodes were left in situ during 10-15 min of baseline recording, followed by intraperitoneal acetate injection. Continuous recording was obtained during 70 min after acetate injection. Mouse movement during injection was minimized by securing tubing position with adhesive tape at multiple points inside a Faraday cage.

In vivo neurophysiological data analysis

Neurophysiology analysis was conducted offline with programs written in MATLAB.

Power spectral density, an index of spontaneous summed synaptic activity, was generated for delta (< 4 Hz), theta (4 – 7 Hz), alpha (7 – 14 Hz), beta (15 – 30 Hz) and low gamma (30 – 50) frequency bands using a fast Fourier transform for every 5 s segment of a 30 min (mouse spontaneous LFP) or a 25 min (human EEG) recording. The average power spectra of 360 segments (mouse spontaneous LFP) or 300 segments (human EEG) were calculated.

Coherence (C_{xy}), an index of functional connectivity between layer 2 and layer 4 co-recordings (mouse spontaneous LFP) or between EEG electrodes (human EEG) was expressed as magnitude squared coherence using Welch's averaged modified periodogram method with the formula:

$$C_{xy}(f) = (|P_{xy}(f)|^2) / P_{xx}(f)P_{yy}(f)$$

where $P_{xx}(f)$ and $P_{yy}(f)$ are the power spectral densities for each of the two signals $x(t)$ and $y(t)$ occurring at time (t) and $P_{xy}(f)$ is their cross spectral density. Coherence is the frequency domain analog of the correlation coefficient in statistics. It indicates the degree of coupling of two signals at each frequency, with 1 indicating perfect coupling. Coherence was calculated for each 5 s segment of a 30 min (spontaneous mouse LFP) or a 25 min (human EEG) recording and averaged across all 5 s segments to determine a value for that mouse or human subject.

Evoked LFP. The amplitude of evoked LFPs was measured from 0.3 to 50 ms after stimulation and the average of 5 evoked LFPs for each stimulus strength used as the response. For stimulation trains, the window used to calculate maximum response for interstimulus intervals of 5, 1, 0.5, 0.1, 0.05 and 0.025 s was 50, 50, 50, 50, 49 and 24 ms respectively. Paired pulse ratios were estimated by dividing the mean response to the 2nd-6th stimuli in a train by the response to the first stimulus in that train. For acetate modulation experiments, baseline measurements included from -10 to 0 min immediately prior to acetate injection, and acetate +1 hr measurements included from 60 to 70 min after acetate injection.

Extracellular multiunit action potentials (spikes) were detected as positive or negative voltage deflections that were 7 times greater than the median absolute deviation of a voltage recording (64). To avoid multiple detections of the same spike, a “detector dead time” of 1.5 ms followed each spike detection. Spikes were sorted into single units using MATLAB Toolbox “Wave_Clus” (64) for semi-automated clustering and sorting of single units. The average waveform of a single unit was analyzed to determine half-width (width in μ s of the action potential at half its maximum amplitude) and spike-width (distance in μ s between positive and negative peaks) (fig. S9E). The shape of single units has been used to classify action potentials as originating from putative pyramidal excitatory or putative, parvalbumin-containing inhibitory neurons (44–46). Single units were classified as broad spike (RS, putative excitatory pyramidal

neurons) or narrow spike (FS, putative parvalbumin fast-spiking inhibitory neurons) in a half-width relative to spike-width plot using κ -medoid clustering. As in previous studies, further support for the classified narrow spikes as originating from putative inhibitory neurons was provided by a decrease in the probability of firing of neighbor neurons with the occurrence of a narrow spike in control mice (fig. S10). Epileptiform activity detection amongst spontaneous action potentials was achieved by manual detection of the beginning and end of a burst of action potentials in each 30 s segment of a spontaneous, uninterrupted 30 min recording by an observer blind to the control or PDHD mouse source of the trace. Action potential bursts > 3 s were considered epileptiform.

EEG

Human: Scalp video-EEG recordings were obtained from healthy children and patients with PDHD using a standard 10-20 electrode placement system referenced to an average configuration. An uninterrupted seizure-free 25 min period of quiet wakefulness was selected for analysis. For each 5 s segment of analyzed EEG, any movement artifact resulted in the removal of that segment from all channels prior to further analysis. EEG spectral power and coherence analysis was conducted as described above for mice.

Mouse: Mice aged P21-P25 were used for semiacute EEG recordings. After inducing anesthesia by inhalation of 1-2% isoflurane in a 1 L/min mixture of 70% nitrous oxide and 30% oxygen, two epidural recording electrodes (#00-90 \times 1/8 inch stainless steel screws) were placed (anteroposterior position -1.0 mm, lateral \pm 1.5 mm from bregma), along with a reference and ground screw over the olfactory bulb and cerebellum, respectively. Electrodes were attached via flexible wire (kynar 30 awg) to a custom 6-pin micro-connector (Omnetics) and secured with dental acrylic resin. Buprenorphine (0.05 mg/kg of weight) was administered following surgery.

Mice were allowed to recover for at least 2 hr prior to EEG recording. Recordings were performed in a custom acrylic cage (Marsh Designs) adjacent to a RZ2/PZ3 neurophysiology workstation (Tucker-Davis Technologies). A flexible cable suspended from the top of the mouse cage was fitted with an interposed commutator to minimize mouse restraint. EEG recordings (300 Hz sampling) were analyzed by a researcher blinded to genotype.

Whole cell patch clamp slice recording

Brain slice preparation: Recording from viable cells from PDHD mice brains was not practicable with commonly used protocols, as massive cell loss was noted under standard dissection and recovery solutions, with all slices displaying early cell swelling, diffuse cell borders and visible nuclei. This included the following additions or procedures, undertaken singly or in combination: a) glucose 10 mM in recovery artificial cerebrospinal fluid (ACSF); b) acetate 10 mM (instead of glucose) in ACSF; c) 2-Amino-5-phosphonopentanoic acid (AP-5, 100 μ M) and cyanquixaline (CNQX, 20 μ M) in dissection buffer; d) ascorbate (5 mM), thiourea (2 mM) and pyruvate (3 mM) in recovery ACSF; e) use of younger mice (P16 instead of P21-P25); f) use of ketamine prior to decapitation and addition of N-Methyl-D-glucamine (NMDG, 93 mM) to dissection buffer; g) transcardial perfusion with chilled NMDG buffer; h) a combination of AP-5 (100 μ M) and CNQX (20 μ M) in dissection buffer, plus ascorbate (5 mM), thiourea (2 mM) and pyruvate (3 mM) in recovery ACSF using P16 mice. Viable cortical brain slices (400 μ m) were successfully prepared from 16-18 day-old PDHD mice and littermate controls by combining the following procedures: a) anesthesia, prior to decapitation, with ketamine (100 mg/kg) and xylazine (25 mg/kg); b) transcardiac perfusion with chilled (4°C) dissection buffer; c) addition of NMDG (93 mM) to the dissection buffer instead of sucrose; d) slice recovery and recording at room temperature; e) use of dissection buffer containing (in

mM): 93 NMDG, 2.5 KCl, 1.2 NaH₂PO₄, 30 NaHCO₃, 20 HEPES, 10 D-Glucose, 0.5 CaCl₂ and 5 MgSO₄, aerated with 95% O₂/5% CO₂. The elevated Mg²⁺/Ca²⁺ (10:1) ratio in the buffer was intended to dampen synaptic transmission, neuronal activity and potential glutamate excitotoxicity. A Leica VT 1200S vibratome was used to produce coronal slices bathed in chilled dissection buffer. PDHD mouse cells did not survive above room temperature; therefore slices were recovered at room temperature in ACSF. Recovery and baseline recording ACSF contained (in mM): 118 NaCl, 2.5 KCl, 26 NaHCO₃, 1.25 NaH₂PO₄, 2 CaCl₂, 2 MgSO₄ and 10 D-Glucose. The solution was aerated with 95% O₂/5% CO₂ to pH 7.4. Picrotoxin (100 μM) was then freshly dissolved prior to use to record predominantly glutamatergic currents. Acetate experiments were conducted after adjusting ACSF solute composition to accommodate 5 mM acetate as a sodium salt (C₂H₃NaO₂) to maintain sodium electrochemical driving force (65). The acetate-ACSF solution contained (in mM): 113 NaCl, 2.5 KCl, 26 NaHCO₃, 1.25 NaH₂PO₄, 2 CaCl₂, 2 MgSO₄ and 5 C₂H₃NaO₂. All reagents were purchased from Sigma-Aldrich.

Electrophysiology: Slices were allowed to recover for at least 2.5 hours (66) before transfer to the recording chamber. There, they were perfused with ACSF containing picrotoxin (100 μM) at 2.5-3 ml/min at room temperature. Cells were visualized using differential interference contrast optics with an Eclipse FN1 microscope (Nikon). Narrow pipette tips with resistance 10 – 20 MΩ delay intracellular dialysis and do not impact intracellular currents for up to 20 minutes (67). Thus, we used pipette tips with 14-20 MΩ resistance. They were filled with a pH 7.2, 285 mOsm solution containing (in mM): 125 K-gluconate, 2.6 KCl, 1.3 NaCl, 10 HEPES, 0.1 EGTA and 15 sucrose. A > 4 GΩ seal was obtained on cortical layer IV/V neurons while voltage clamping at -65 mV, followed by alternating 50-100 μs, 1 V pulses with strong and brief suction to break through the cell membrane. The resting membrane potential was immediately noted and gentle suction was then maintained for 10-15 s to prevent resealing. In current clamp mode, voltage

responses and action potentials were elicited in response to 600 ms current steps from -250 pA to 350 pA in 25 pA increments. The large current step to first elicit an action potential was noted, followed immediately by small current steps in 2.5 pA increments in a current range that bracketed the noted large current step to determine rheobase. This established baseline excitability and was completed within 3 min of intracellular access. If the experiment involved further recording, the cell was voltage clamped at -65 mV and series resistance compensated (40 – 60 %) to maintain it at 20 – 35 M Ω . Baseline input resistance in current clamp mode was calculated offline from the slope of voltage responses (550 to 600 ms after current step start) to sub-threshold current steps (from -100 pA to -25 pA below rheobase). Spontaneous excitatory post synaptic currents (sEPSCs) were recorded for the next 12 min. The first 5 min was analyzed for baseline sEPSC frequency and amplitude. Subsequently, ACSF was switched to solution containing 5 mM sodium acetate. After a 2 min interval, the next 5 min of recording was analyzed for sEPSC frequency and amplitude. To minimize the impact of any reduction of voltage clamp across dendrites and synapses due to elevated pipette resistance, we limited analysis of sEPSCs to a single cell for before and after acetate comparisons rather than for comparisons across mice or genotypes. Cells were voltage clamped at -65 mV throughout the recording. Every 2 min throughout the recording session, series and input resistance were monitored in voltage clamp mode using a 600 ms, -10 mV step from holding potential -65 mV (filtered at 20 kHz and sampled at 100 kHz). Data were not analyzed if cell series resistance varied by more than 25 % during the experiment. Spontaneous excitatory post-synaptic events (sEPSCs) were identified offline with Minianalysis (Synaptosoft). The root-mean-square of baseline noise (in pA) was calculated and multiplied by 3 to provide the detection threshold to the automatic program. This was followed by direct scrutiny of each program-detected event

before it was confirmed or excluded as a sEPSC. The detection threshold was constant for each cell recording.

Neuron discharges (fig. S11A) were preliminarily classified based on: a) neuron appearance: broad spike cells typically display pyramidal shapes with an apical dendrite, whereas fast-spiking neurons are oval or spherical without an apical dendrite; b) for a current injection above action potential threshold, broad spike neurons exhibit adaptation of spike frequency, while fast-spiking neurons display minimal or no adaptation; c) fast-spiking neurons demonstrate a higher firing frequency; d) fast-spiking neuron action potential width is narrower and e) fast-spiking neuron action potential exhibits higher amplitude and briefer after-hyperpolarization.

Machine learning protocol

EEG recordings were examined using a data-driven machine learning algorithm designed for seizure prediction. All analyses utilized the MATLAB Statistics and Machine Learning Toolbox using functions and script examples available from the company. MATLAB functions included *fitcsvm* (which trains or cross-validates a support vector machine model for 2-class (binary) classification) with its '*OptimizeHyperparameters*' option selected, and *perfcurve* (for receiver operating characteristic curves or other performance curves for classifier outputs).

Spectral features: This group included: Preictal mouse or human EEG segments analyzed for power in a) delta (0–4 Hz), b) theta (4–8 Hz), c) alpha (8–15 Hz), d) beta (16–30 Hz) and e) gamma (30–50 Hz) bands. In addition, human EEG features included relative gamma power (gamma power relative to total power).

Temporal features: Preictal mouse or human EEG segments analyzed for changes in gamma power as a ratio (power from EEG immediately preceding an epileptiform discharge as

numerator) for mice (from -240 to -210 or -60 to -30 s prior to an epileptiform discharge) or for human subjects (for example, from -210 to -180 s prior to an epileptiform discharge). For randomly selected EEG segments, the change in gamma power across similar time periods (for example across 30 s) was also determined.

Preprocessing, feature selection and avoidance of overfitting bias: The values of EEG spectral features lie within varying dynamic ranges characteristic for each channel. To compare across channels while capturing potential preictal changes, each preictal feature value was normalized to that of a randomly selected 30 s interictal EEG segment from the same channel. If there was more than one randomly selected interictal segment in a channel, their average was utilized for normalization. These segments occurred at least 4 min preceding or succeeding an epileptiform discharge. The number of total randomly-selected interictal segments for each mouse was equal to the number of total preictal segments in that mouse. Although classifier performance improves with a greater number of features, choosing too many features, especially for smaller training sets, can lead to data overfitting; in other words, the classifier can accurately detect the subset of preictal events used for training while failing to detect the subset of preictal events used to test the classifier. Hence, the number of spectral features for preictal detection in PDHD was limited to those identified as different between PDHD and control by prior analysis. The temporal feature was limited to one spectral feature (gamma power). Overfitting was further avoided by 10-fold cross-validation. This was accomplished by partitioning the dataset (including all preictal and random segment values) into 10 equal sized subsamples. One subsample was set aside as validation data for model testing whereas the remaining 9 subsamples were used for training. The ability of the trained classifier to correctly classify the validation data was evaluated from the proportion of misclassified observations detected on the subsample that was set aside. The

process was repeated by setting aside the other subsamples in 9 more iterations. The average misclassification rate for the 10 iterations was used as a measure for each dataset.

Support vector machine (SVM) classifier and hyperparameter optimization: SVM classifiers utilize decision planes that define decision boundaries. A decision plane separates feature values of a class from those of another. The SVM classifier computes the hyperplane that maximizes the separation margin between classes. The shape of the decision boundary was presumed linear (using a linear kernel), gaussian (using a gaussian or radial basis function kernel) or polynomial (using a polynomial kernel of 2nd, 3rd or 4th order). To find the optimal kernel, a cross-validated SVM classifier was subjected to Bayesian optimization by cycling through different kernels, with 10-fold cross-validation for each cycle determining the performance for that cycle (i.e., computing the misclassification rate). The kernel that yielded the best classification was employed. In addition to kernel function, other hyperparameters that were optimized included kernel scale (a hyperparameter that determines level of smoothing of the kernel; in other words, a higher scale considers a narrower region of points near the decision boundary to determine the decision boundary and the resultant boundary curves around each point from the two classes and is less smooth), box constraint (a hyperparameter that manages the maximum penalty placed on margin-violating values and assists in preventing overfitting) and the presence of standardization (normalizing all data by subtraction from the mean and division by standard deviation). Through 30 cycles of SVM classifier and cross-validation, the hyperparameters were successively adjusted to the settings that classified optimally.

Additional methodological assumptions

Interval following ¹³C substrate administration: NMR was performed 1 hr following intraperitoneal injection of ¹³C tracers to satisfy these requirements: a) ensure that most of the

tracer entered the systemic circulation (30-45 min in rodents (68)); b) detect, at high resolution, all metabolites analyzable by NMR, allowing for unequivocal assignment of ^{13}C multiplets; c) achieve or approach isotopomer metabolic steady state. In optimization experiments conducted as previously (48), analyses at 1 hour after substrate injection met these conditions. To reach as much proximity to the metabolic steady state as possible, the glutamate C3/C4 ratio was used. The reason is that, when ^{13}C -glucose and ^{13}C -acetate are oxidized, glutamate C4 is labeled in the first TCA cycle, whereas its C3 and C2 isotopomers are labeled in subsequent cycles (69, 70). If anaplerosis were absent, glutamate C3/C4 would be unity under metabolic steady state. However, brain anaplerotic flux via pyruvate carboxylase and other reactions reaches at least 10% of TCA cycle flux such that the C3/C4 ratio will necessarily be <1 (70, 71). Indeed, the glutamate C3/C4 ratio was constant across experimental groups (control: 0.84 ± 0.02 , PDHD: 0.81 ± 0.03) and approached the values obtained at metabolic steady state under other experimental conditions (69). Continuous intravenous infusions allow for more precise monitoring of content and enrichment of ^{13}C tracers (13), but were unfeasible given the diminutive size and frailty of PDHD mice.

Acetate dose: The injections used in NMR experiments contained the minimum amount of ^{13}C acetate that produced ^{13}C NMR spectra of sufficient quality for isotopomer analysis. In contrast with other reported plasma acetate concentrations (3-18 mM (72-74)), optimum quality NMR spectra were obtained with 1-2 mM plasma acetate. To correlate changes in excitability with NMR observations, the same injection concentration and analysis time points were used for in vivo electrophysiological (intracortical and EEG) studies. Similarly, because in brain slices 5 mM acetate robustly contributes to glutamate formation as detected by NMR (65), we used that concentration for brain slice electrophysiological experiments. Lower acetate concentrations (0.4

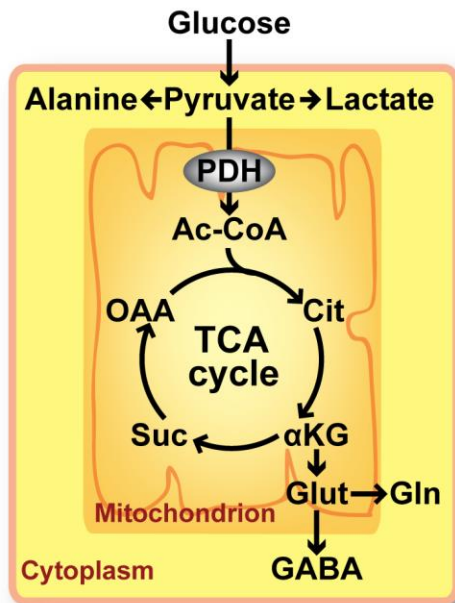
– 0.8 mM, which suppress excitability in hippocampal dentate granule neurons (75)) were not tested.

NMR spectra interpretation: TCA cycle activity was deduced from the doublets D45 (glutamate C4 and glutamine C4) and D12 (GABA C2) and quartets (Q) of all NMR isotopomers by virtue of the mechanism of quartet generation (which requires two complete cycles) relative to doublet formation (accomplished after one cycle). Lower abundance multiplets (doublet D34 in glutamate C4 and glutamine C4, doublet D23 in GABA C2) were assumed to arise from multiple cycles of the tracer through the TCA cycle, and singlets (S) to originate primarily from naturally abundant ^{13}C (amounting to 1.1% of all natural carbon). Because the sum of all the fractional amounts of multiplets must equal 1, any reduction in D34 and quartets in glutamate and glutamine C4, and in D12 in GABA C2 must result in a proportionally greater contribution of singlets to the spectra.

Metabolism of [1,2- ^{13}C]acetate through the first two cycles of the TCA cycle was assumed to label glutamate and glutamine primarily in carbons 4 and 5 (D45) and carbons 3, 4 and 5 (Q), respectively, and GABA in carbons 1 and 2 (D12) and 1, 2, and 3 (Q), respectively. [1,6- ^{13}C]glucose metabolism through the first two cycles was assumed to lead to glutamate and glutamine labeling in carbons 4 (S) and 3 and 4 (D34) and GABA in carbons 2 (S) and 2 and 3 (D23), respectively. Glutamate and glutamine C4 multiplets derived from [1,2- ^{13}C]acetate thus primarily reflected acetate metabolism, whereas those derived from [1,6- ^{13}C]glucose reported primarily glucose oxidation. The enrichment of GABA C2 multiplets relative to glutamate C4 multiplets reflected the metabolism of GABA-producing relative to glutamate-producing cells.

Fig. S1

A



B

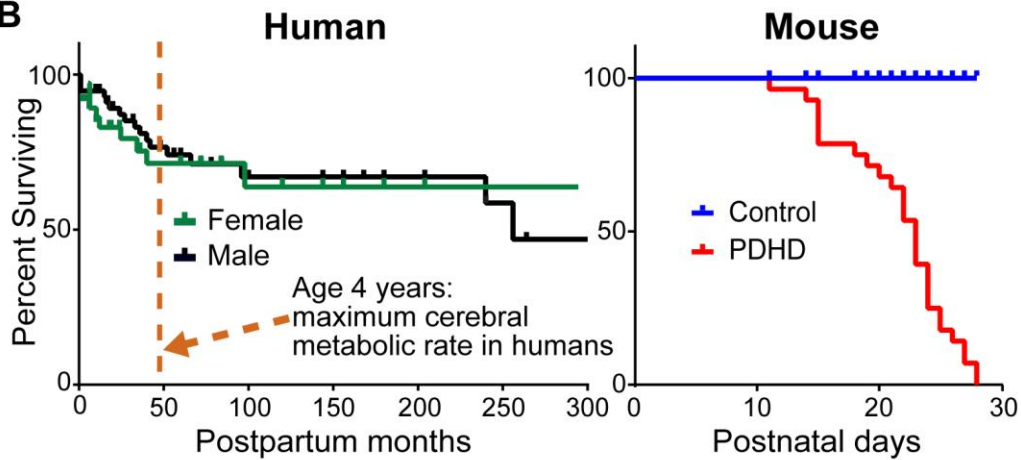


Fig. S1. Glucose metabolism schema and survival curves of patients and mice with PDHD.

(A) Schematic representation of glucose metabolism and neurotransmitter synthesis. Ac-CoA: acetyl-CoA, Cit: citrate, α KG: α -ketoglutarate, Glut: glutamate, Gln: glutamine, Suc: succinyl-CoA, OAA: oxaloacetate

(B) Kaplan-Meier survival curves of patients with PDHD (57 males and 35 females) and of control and PDHD mice (n= 28 males in each group).

Fig. S2

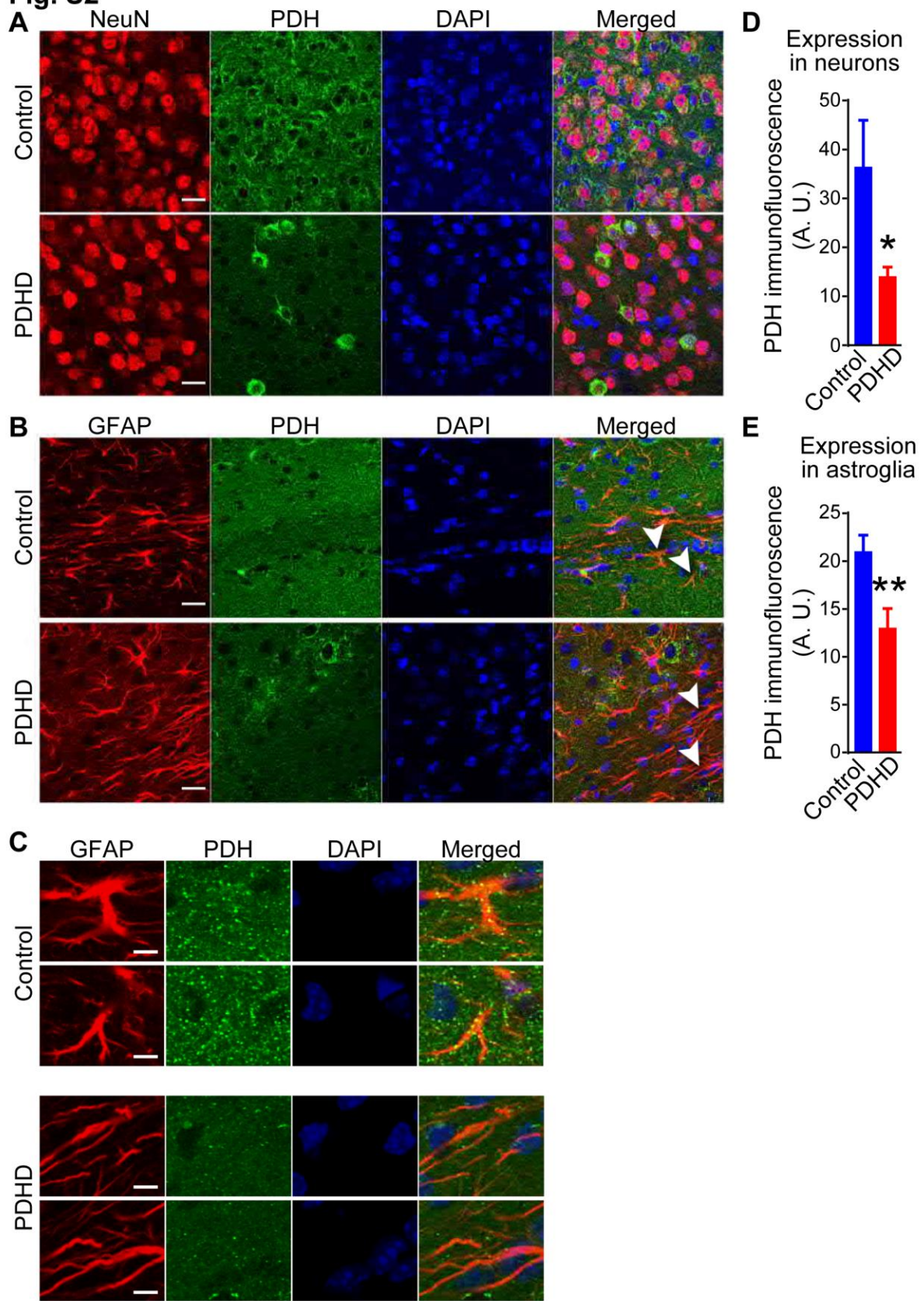


Fig. S2. Expression of PDH in the mouse somatosensory cortex.

(A, B) Coronal cortical sections triple-stained with anti-NeuN (A) or anti-GFAP (B), anti-PDHA1 and DAPI in control and PDHD cortex. Scale bar= 20 μm .

(C) Magnified views to reveal astrocytes in B (arrowheads). Scale bar= 5 μm .

(D, E): Quantification of PDH fluorescence intensity in neurons (D) and astrocytes (E) in cortex.

Values indicate mean \pm S.E.M. Statistical differences were determined using two-tailed

Student's *t* test. *: $p < 0.05$, **: $p < 0.01$.

Fig. S3.

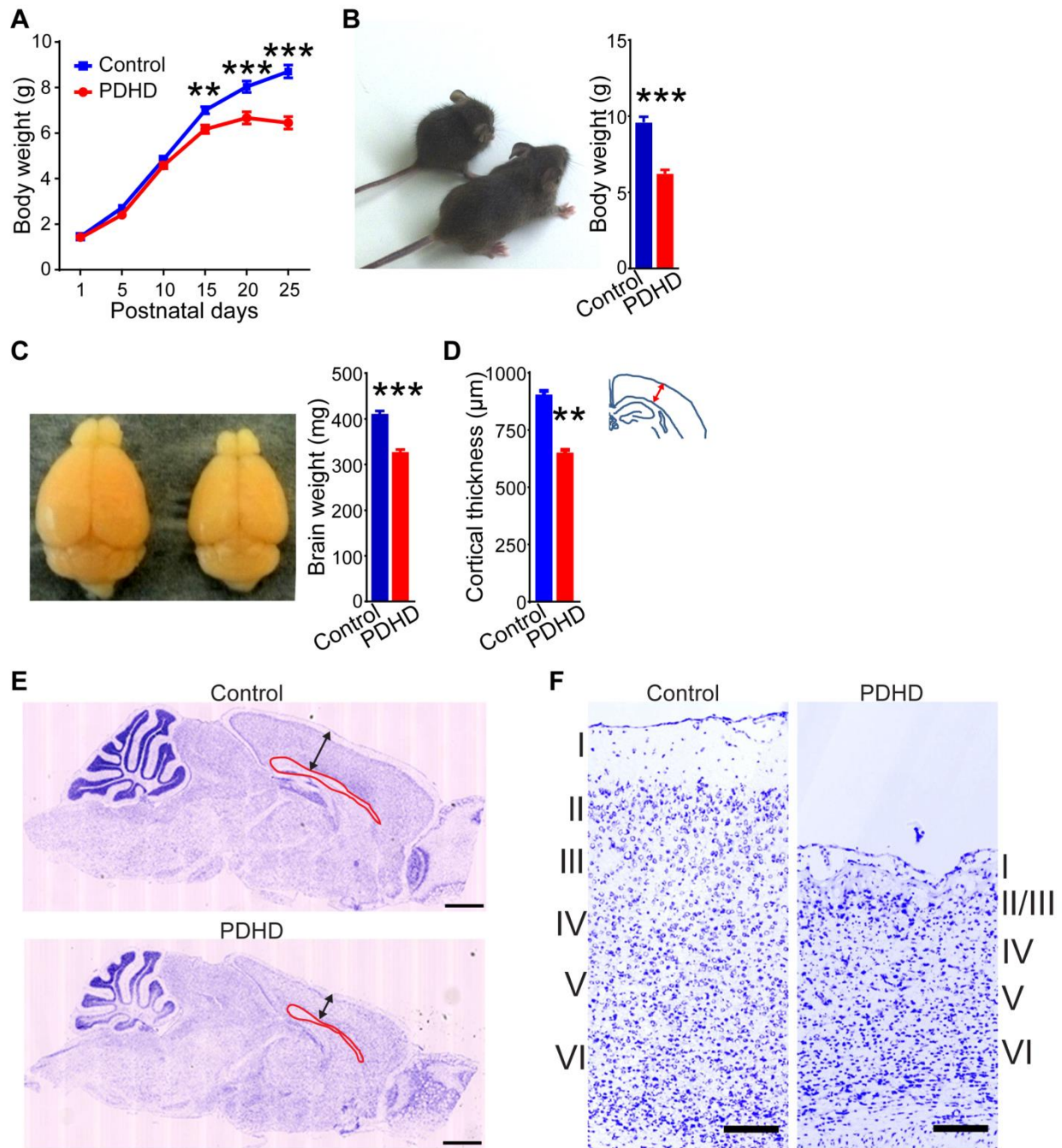


Fig. S3. Phenotype of PDHD mice.

(A) Growth of PDHD and control mice (n= 10 males in each group).

(B-C) Body size, body weight, brain size, brain weight of PDHD mice and control littermates at P23 (n= 10 males in each group).

(D) Cerebral cortical thickness (n=9 slices, 3 per mouse in each group) with schematic coronal section depicting the region measured.

(E) Sagittal brain sections stained with cresyl violet illustrating corpus callosum thickness (red boundary) and the cerebral cortex (double-headed arrow). Scale bar= 1.5 mm.

(F) Somatosensory cortex layers visualized after Nissl staining. Scale bar= 110 μ m.

Values indicate mean \pm S.E.M. Statistical differences were determined using two-tailed

Student's *t* test. **: $p < 0.01$, ***: $p < 0.001$.

Fig. S4.

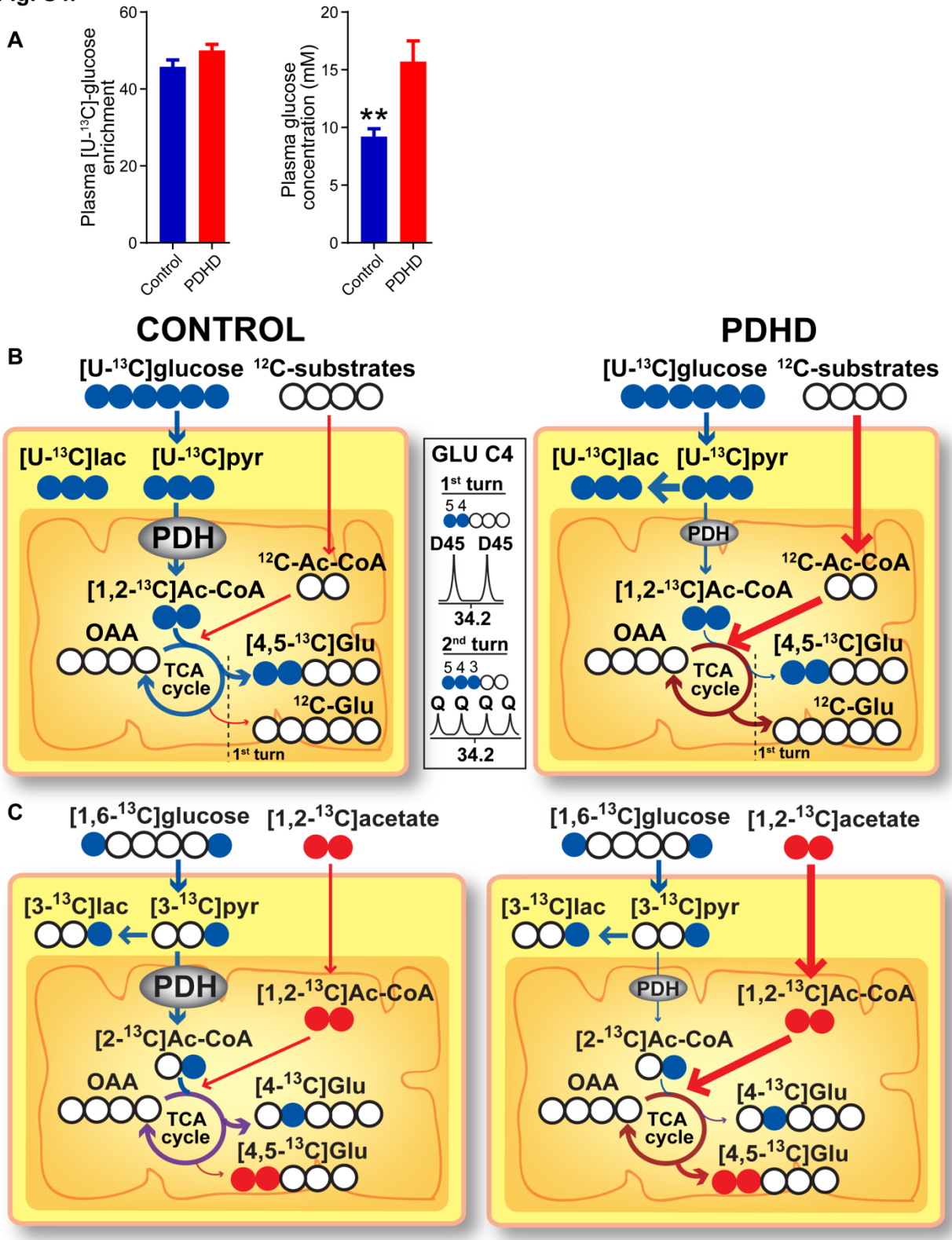


Fig. S4. Glucose metabolism in PDHD mice.

(A) Plasma [U-¹³C]-glucose enrichment and glucose concentration 1 hr after intraperitoneal injection of [U-¹³C]-glucose in control and PDHD mice.

(B) Schema portraying glucose metabolism in control and PDHD mouse cortex. The reduced enrichment of [1,2-¹³C]acetyl-CoA derived from [U-¹³C]glucose in the PDHD cortex (right panel) suggests that alternative, non-labeled substrates are oxidized downstream PDH in the PDHD cortex

(C) Schematic glucose and acetate metabolism in control and PDHD cortex based on the data in panels of Fig. 3A and 3B.

GLU: glutamate, GLN: glutamine, ASP: aspartate, ALA: alanine, GABA: γ -aminobutyric acid, NAA: N-acetyl aspartate, LAC: lactate, ALA: alanine, PYR: pyruvate, Ac-CoA: acetyl-CoA, TCA cycle: tricarboxylic acid cycle. C#: carbon labeled in position. Data indicate mean \pm S.E.M. Differences were determined by a two-tailed Student's *t* test. **: $p < 0.01$.

Fig. S5 Human Subject EEGs

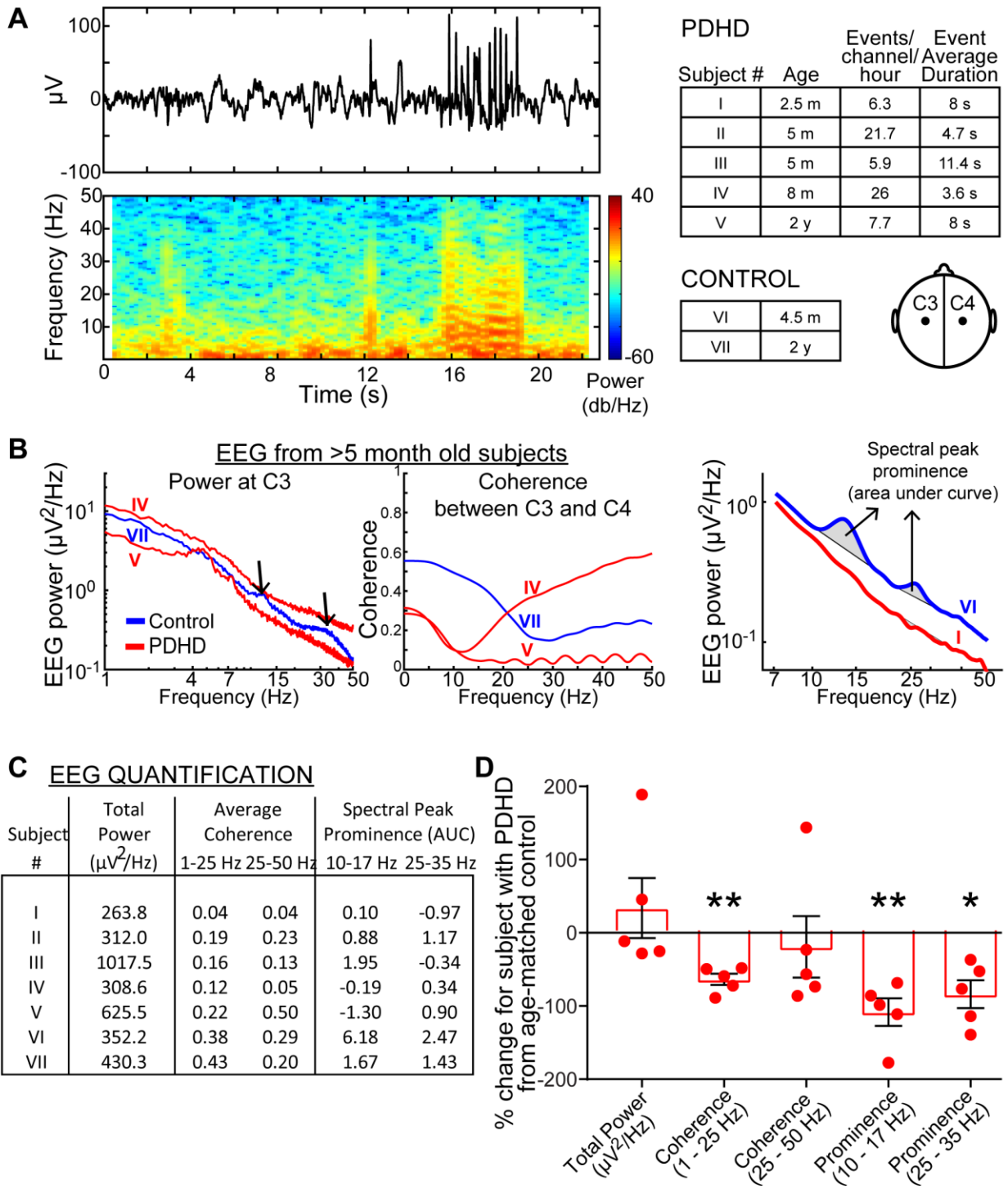


Fig. S5. EEG in patients with PDHD.

(A) *Left* - EEG trace (bandpass filtered 1-50 Hz) from a patient with PDHD illustrating epileptiform activity with a power spectrogram below. *Right* – Age and epileptiform event characteristics of PDHD and control subjects with a schematic diagram depicting the position of EEG electrodes C3 and C4.

(B) *Left and middle panels*: Average EEG power spectra and coherence (average of 5 s segments for a > 25 minute recording) from PDHD (> 5 month old) and control subject. Roman numerals refer to subjects in (A). Black arrow indicates a 10 - 15 Hz and 30 – 35 Hz oscillation peak (black arrow) in control. *Right panel*: Spectral peak prominence in an example EEG power spectra from control contrasted with that of a patient with PDHD. The area under the curve of the peak was assayed as an index of the prominence of a spectral peak.

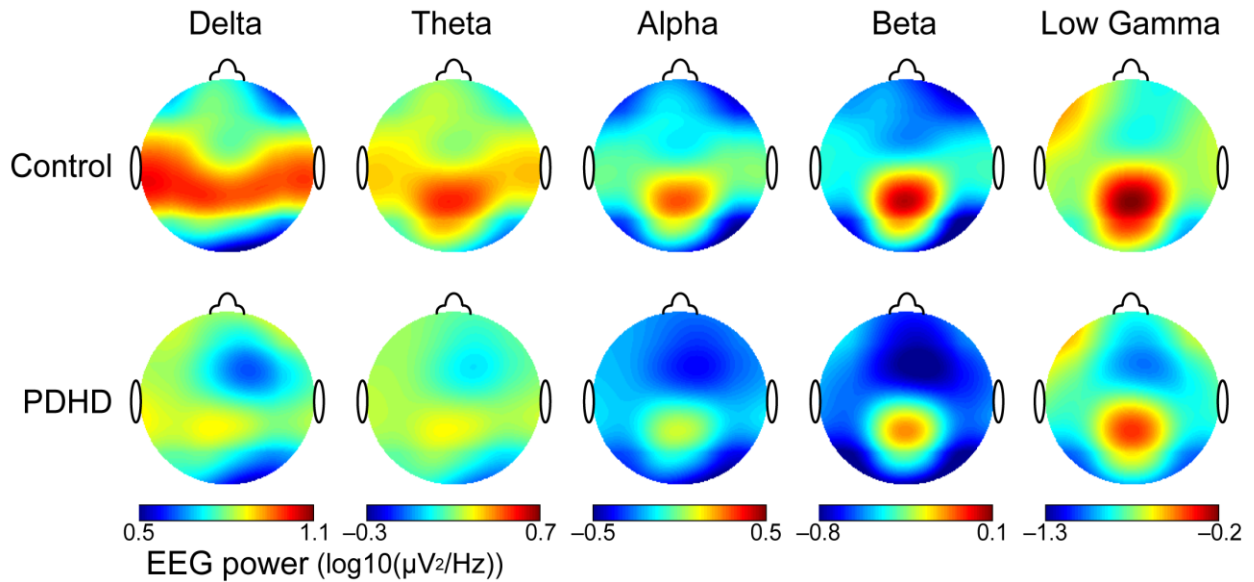
(C) Quantification of EEG total power, average coherence for two frequency bins (1 to 25 Hz and 25 Hz to 50 Hz), and prominence of EEG power spectra for two frequency ranges (10 to 17 Hz and 25 to 35 Hz) for patients with PDHD.

(D) Data of patients with PDHD from fig. S5C depicted as percentage change from age-matched control.

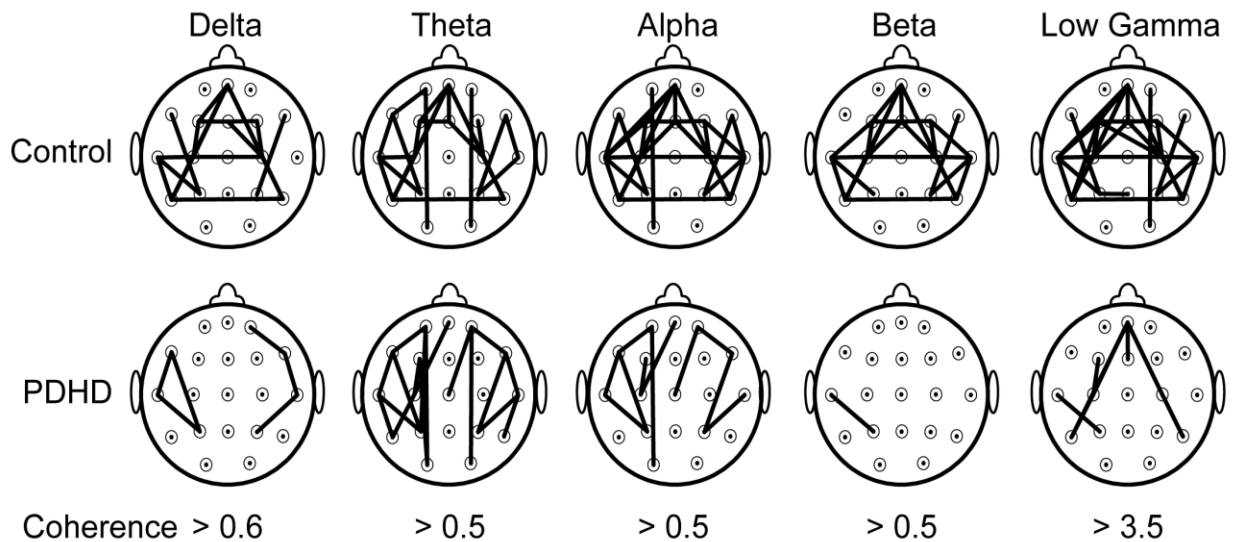
Data in bar plots indicate mean \pm S.E.M. Statistical significance was determined by a one sample t-test testing if the data mean was significantly different from the value of zero with zero representing no change from control. *: $p < 0.05$ **: $p < 0.01$.

Fig. S6

A EEG power (human) for all electrodes



B Coherence (human) between all electrodes



Number of electrode pairs with coherence > threshold

	Delta	Theta	Alpha	Beta	Gamma
Control	19	24	30	25	32
PDHD	6	18	11	1	8

Fig. S6. Patient with PDHD EEG (patient I).

(A) EEG Power: Placement of EEG electrodes is indicated by black dots in the delta frequency bin. Black numbers indicate mean EEG power referred to the corresponding electrode channel.

EEG power at scalp points between electrodes was calculated using 2-D spline interpolation. The color code corresponding to EEG power at any point is given below each frequency bin.

(B) Coherence: EEG electrode positions are indicated by black circles. Straight lines between two electrode positions indicate that coherence (a measure of functional connectivity) between the two electrode channels exceeds the threshold given below. Quantification of the number of electrode pairs above the threshold is given in the table at the bottom.

Fig. S7 Human Subject EEGs

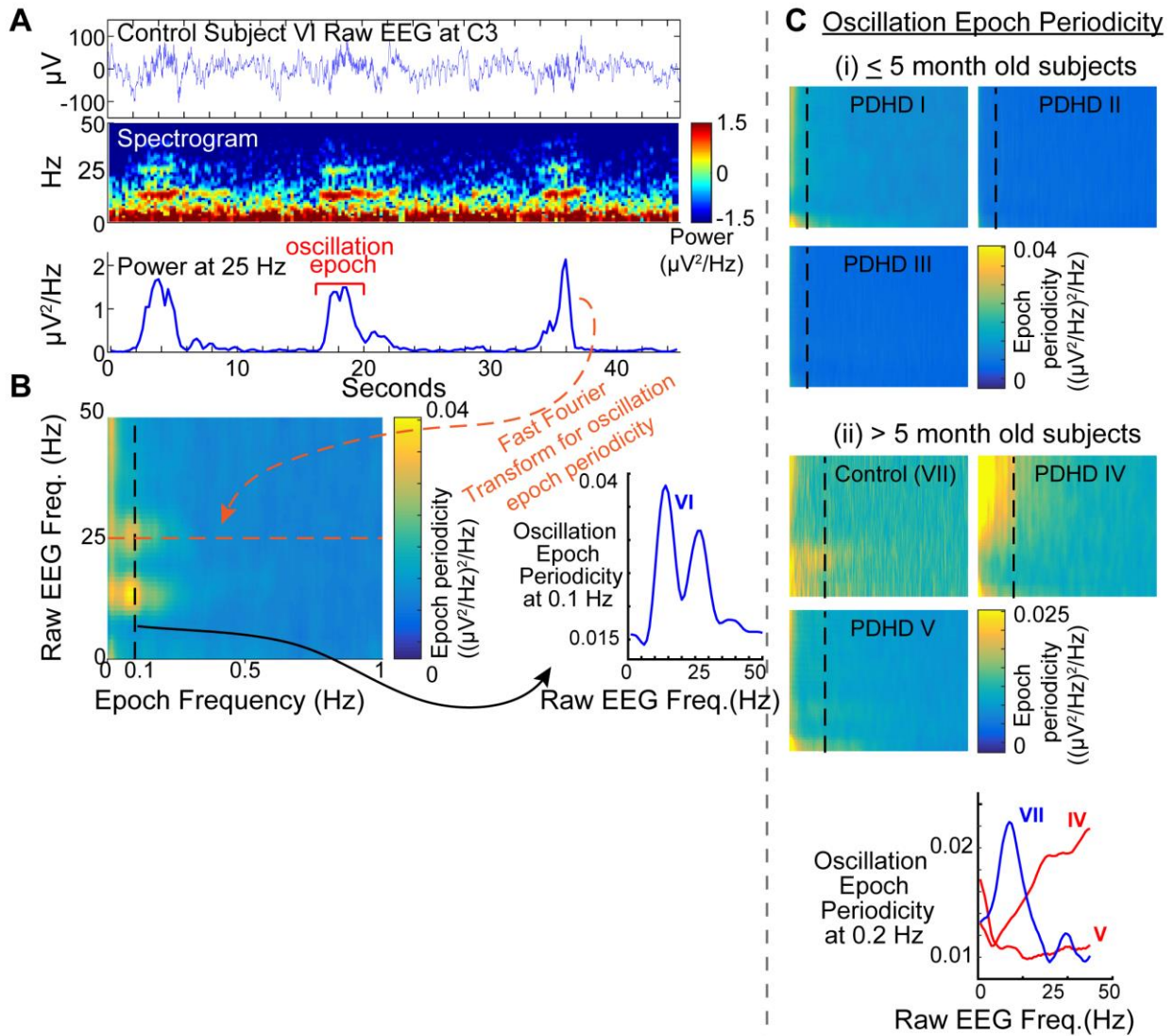


Fig. S7. EEG oscillation epochs in patients with PDHD.

(A) Gamma oscillation epoch in a control subject. *Top and middle* – Unmodified EEG trace and associated spectrogram (below) illustrating transient beta and gamma frequency bursts or epochs that occur periodically every 10 - 12 s. *Bottom* – Power across time derived from the spectrogram at 25 Hz re-plotted as a line to reveal the periodicity of a 25 Hz (gamma) oscillation

epoch. This line has undergone a fast Fourier transformation to further illustrate the periodicity of the 25 Hz oscillation epoch in fig. S7B.

(B) Oscillation epoch periodicity in a 4.5 month old control subject. Left – The power in each unmodified EEG frequency across time (as in the (C) spectrogram) was subject to a fast Fourier transformation to derive oscillation epoch periodicity. ~12 Hz and ~26 Hz EEG oscillation epochs occur every ~10 s (0.1 Hz). Right – Re-plotting of data at 0.1 Hz as a line illustrating distinct peaks for ~12 Hz and ~26 Hz raw EEG oscillations. This line is plotted as an inset together with age-matched PDHD subject data in Fig. 4A for comparison.

(C) Oscillation epoch periodicity. (i) Oscillation epoch periodicity for 2.5 to 5 month-old PDHD subjects and a control subject. (ii) Oscillation epoch periodicity for a 2 year-old control subject and > 5 month old subjects with PDHD.

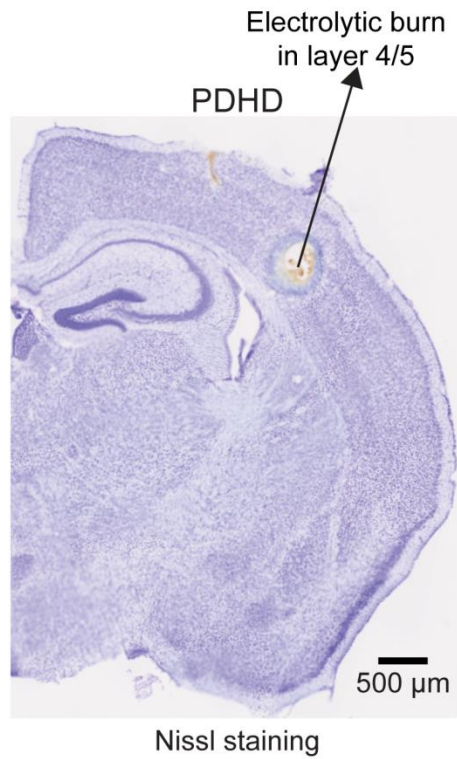
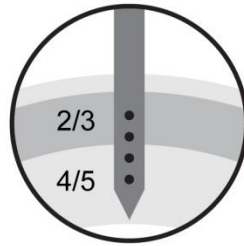
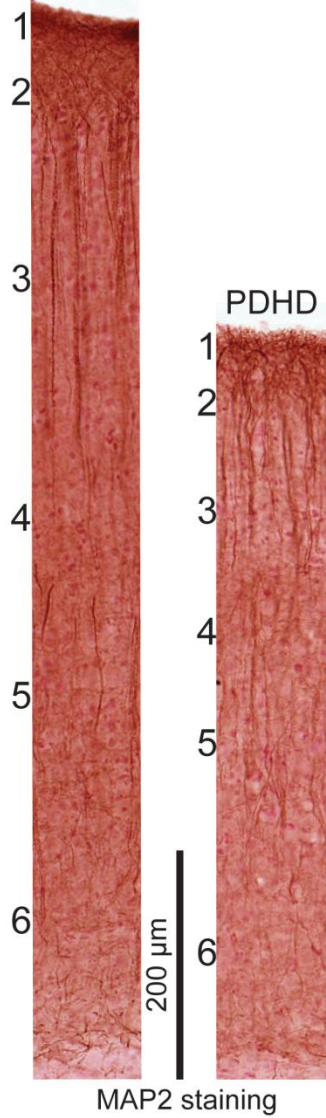
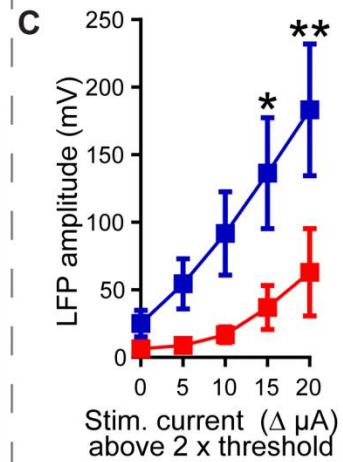
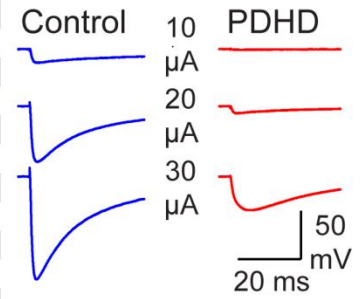
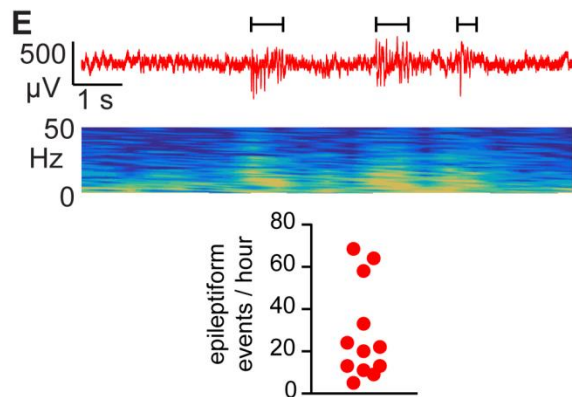
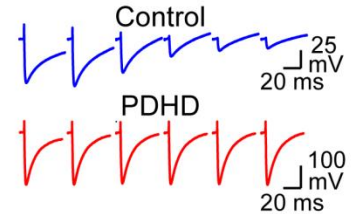
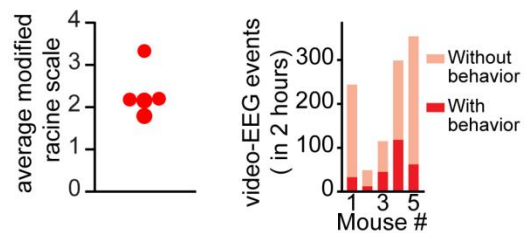
Fig. S8**A** Control**B** Intracortical evoked LFP recording**D** 50 ms interstim. interval**F** Mouse video-EEG

Fig. S8. Cortical layering, evoked LFP, and baseline EEG in PDHD mice.

(A) MAP2 staining in PDHD revealing layer stratification with dendrites extending from layer 2/3 to layer 4/5. Nissl staining helped confirm electrode position in layer 4/5.

(B) Intracortical evoked LFP traces in PDHD and control mice under similar stimulation currents.

(C) Comparison of evoked LFP responses above twice threshold (defined as the minimum stimulation current that evoked a response). The stimulation current level twice above threshold was reassigned a value of zero to restrict comparison only to responding synapses. This comparison minimizes the effect of passive membrane properties that could be impacted in PDHD and prevent some stimulation currents from eliciting a response.

(D) LFP responses to intracortical stimulation trains in control and PDHD mice.

(E) *Top* – Epileptiform tracings in an awake PDHD mouse seen in an EEG recording. Black lines above the trace indicate region of EEG considered as epileptiform event *Bottom* - Epileptiform event frequency detected by EEG from awake PDHD mice.

(F) Behavior-associated EEG epileptiform events in PDHD mice additionally studied with video-EEG. *Left* – average modified Racine score in mice studied with video-EEG recordings. See Table S6 for mouse behavioral features used for scoring with the modified Racine scale. *Right* – Proportion of behavior and non-behavior associated EEG epileptiform events in PDHD mice studied with video-EEG recordings

Values indicate mean \pm S.E.M. Statistical differences were determined using two-tailed Student's *t* test. *: $p < 0.05$; **: $p < 0.01$.

Fig. S9

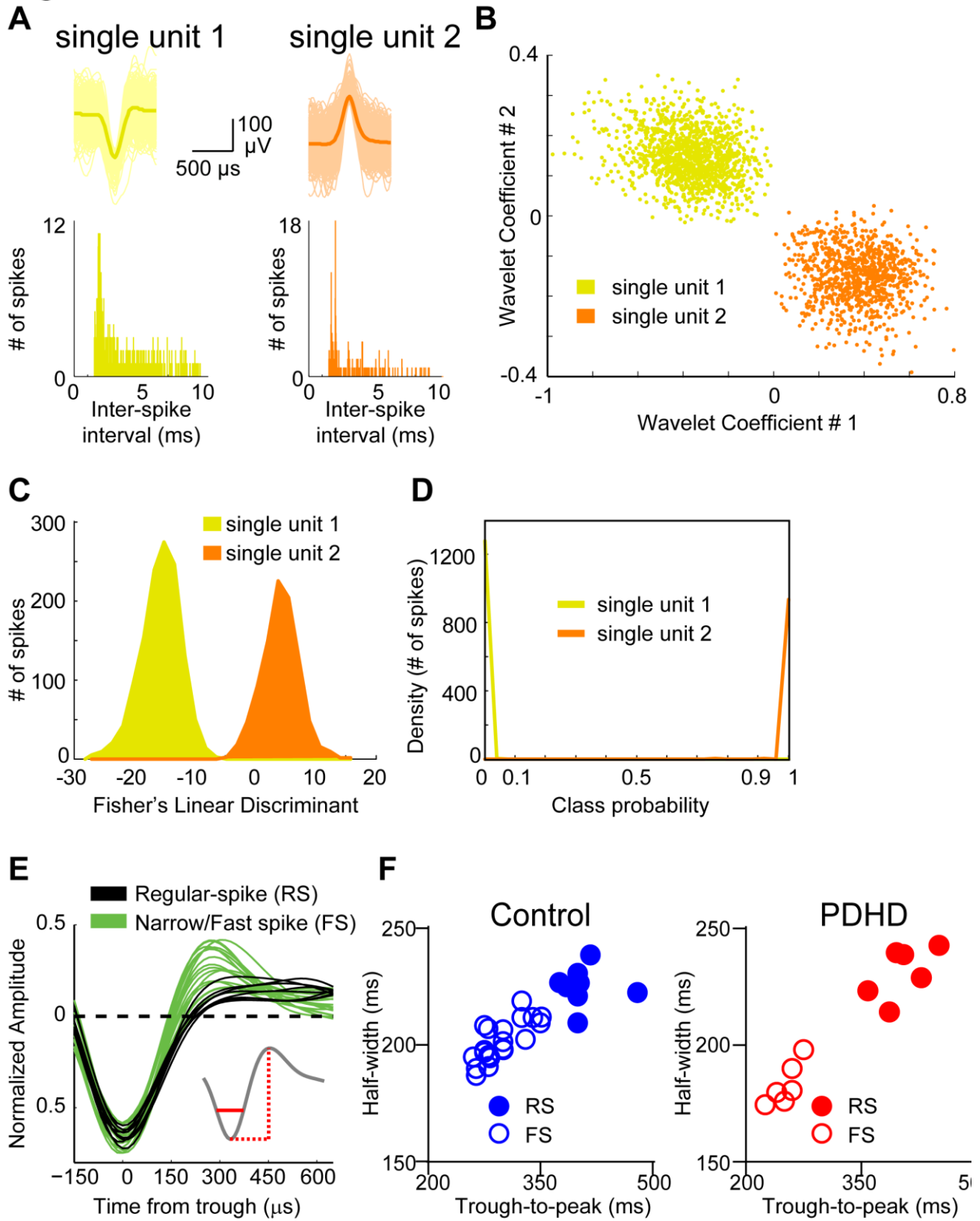


Fig. S9. Sorting of multiunit action potentials into single units and separation into broad- and fast-spiking neuronal origin.

(A) Single-unit spike waveforms (above) sorted using Wave_Clus (see Methods) with interspike interval histogram (below). In each action potential recording plot, a representative spike (darker color) is superimposed on 500 spikes (lighter color).

(B) Projection of spike shapes onto the feature space of wavelet coefficients to reveal distinct clusters for grouping of similarly-shaped waveforms.

(C) Histogram of the projection of each cluster in Supplementary Fig. 5b onto Fisher's linear discriminant.

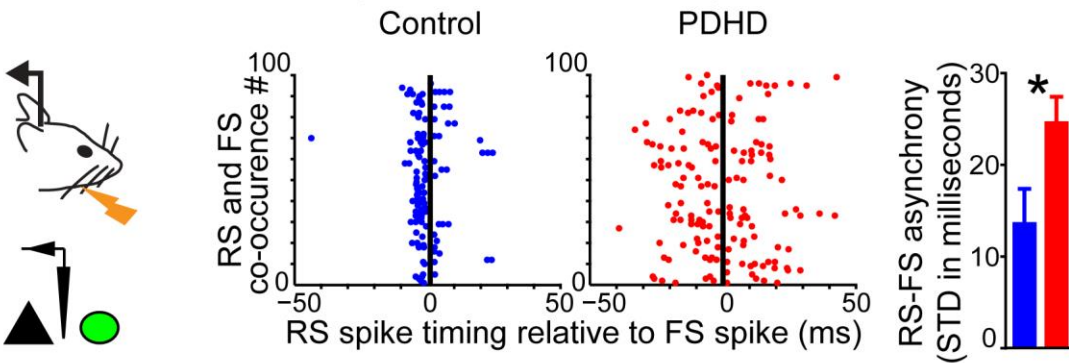
(D) Class probability histogram outline (calculated from linear discriminants in Supplementary Fig. 5c) for either single-unit belonging to the single-unit 2 pool of linear discriminants.

(E) Broad-spike and narrow-spike waveforms from control mice separated from single-unit waveforms using an unbiased unsupervised cluster separation algorithm. Inset - The parameters used for plotting clusters and separation were single-unit trough-to-peak time (dotted red line) and half-width time (solid red line).

(F) Control and PDHD single-unit waveform trough-to-peak and half-widths. Separation into broad-spike and narrow-spike categories used by κ -medoid cluster analysis.

Fig. S10

A *in vivo* extracellular regular- and fast-spike firing



B

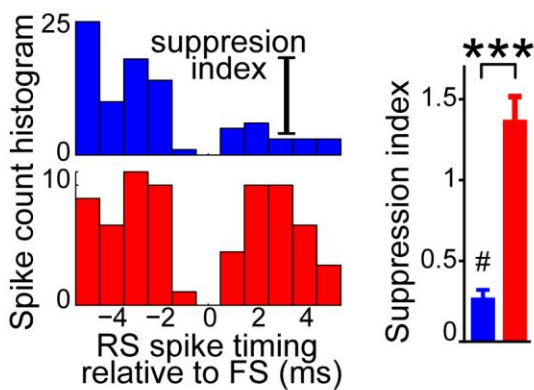


Fig. S10. In vivo RS neuron discharge relative to fast-spiking activity.

(A) *Left* – Example recording from a regular-spike (RS) and a fast-spiking (FS) neuronal pair.

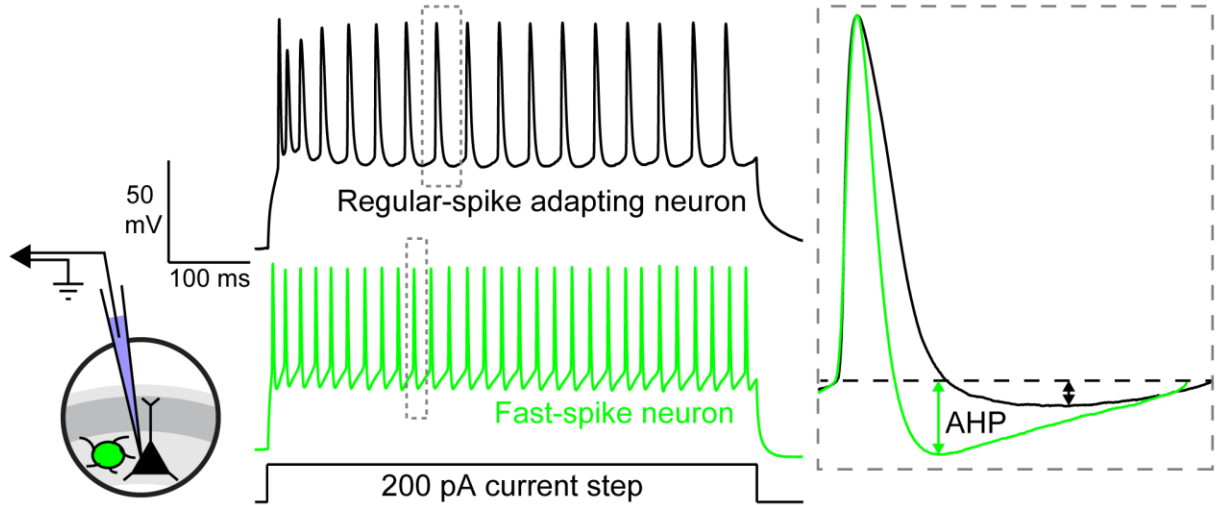
Right – Group data for RS-FS asynchrony in PDHD (n=10 RS-FS pairs) compared to control (n=4 RS-FS pairs).

(B) *Left* – Example RS-FS pair cross-correlogram of dot rasters in Fig. S7A. *Right* – Group data of suppression index in PDHD (n= 10 RS-FS pairs) compared to control (n= 4 RS-FS pairs). The suppression index refers to the number of spikes (in a 5 ms window) immediately after zero divided by the number of spikes (in a 5 ms window) immediately before zero.

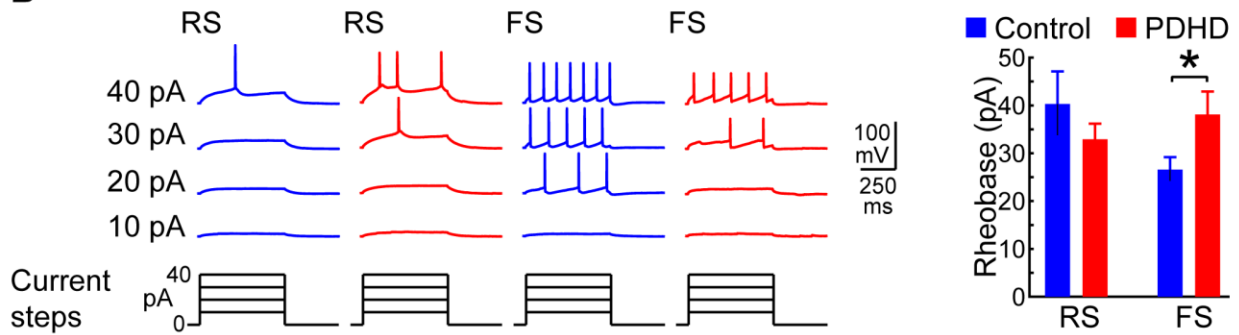
Values indicate mean \pm S.E.M. Statistical differences were determined using two-tailed Student's *t* test. *: $p < 0.05$; ***: $p < 0.001$; # $p < 0.05$ (statistical significance was determined with a one sample t-test testing if the data mean was significantly different from the value of 1, with 1 representing lack of suppression).

Fig. S11

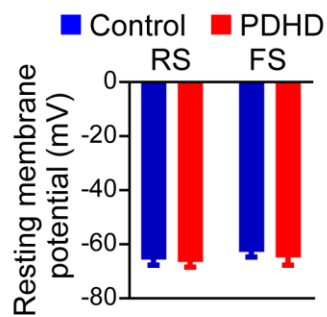
A *ex vivo* intracellular whole cell patch-clamp recording



B



C



D

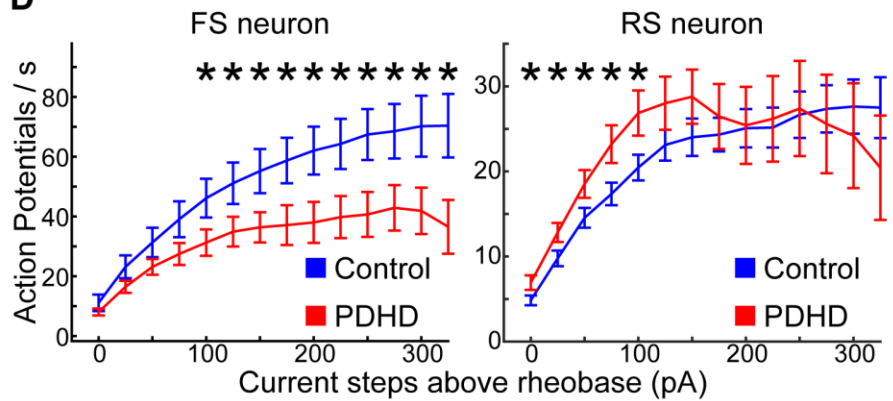


Fig. S11. Brain slice intracellular recordings illustrating cell discrimination, rheobase, and firing.

(A) Narrow-tip (high-resistance) whole cell patch-clamp recording from a control regular-spike adapting (black) and fast-spike (green) neuron.

(B) *Left*: Example responses of control (blue) and PDHD (red) regular-spike adapting (RS) and fast-spiking (FS) neurons to current steps 10 to 40 pA. Compared to control, PDHD regular-spike and fast-spiking neurons require less and more current, respectively, to elicit an action potential. *Right*: Population average rheobase illustrating current required to fire the first action potential (Fast-spiking neurons, control: n= 8 cells, 7 mice; PDHD: n= 17 cells, 15 mice. Regular-spike adapting neurons, control: n= 17 cells, 12 mice; PDHD: n= 23 cells, 16 mice).

(C) Resting membrane potential for regular-spike adapting (Control- n=16 cells, 12 mice; PDHD – n=21 cells, 16 mice) and fast-spike neurons (Control: n = 8 cells, 7 mice; PDHD: n =18 cells, 14 mice) in whole-cell patch clamp recordings from control and PDHD mice cortical slices.

(D) Population averages of action potential numbers elicited by current steps above rheobase (rheobase= minimum current evoking an action potential and in this figure, represented by current step 0) in fast-spiking neurons (control: n= 9 cells, 7 mice; PDHD: n= 17 cells, 13 mice) and regular-spike adapting (control: n= 22 cells, 12 mice; PDHD: n= 26 cells, 15 mice).

Values indicate mean \pm S.E.M. Statistical differences were determined using two-tailed Student's *t* test. *: $p < 0.05$.

Fig. S12

Input resistance with cell dialysis

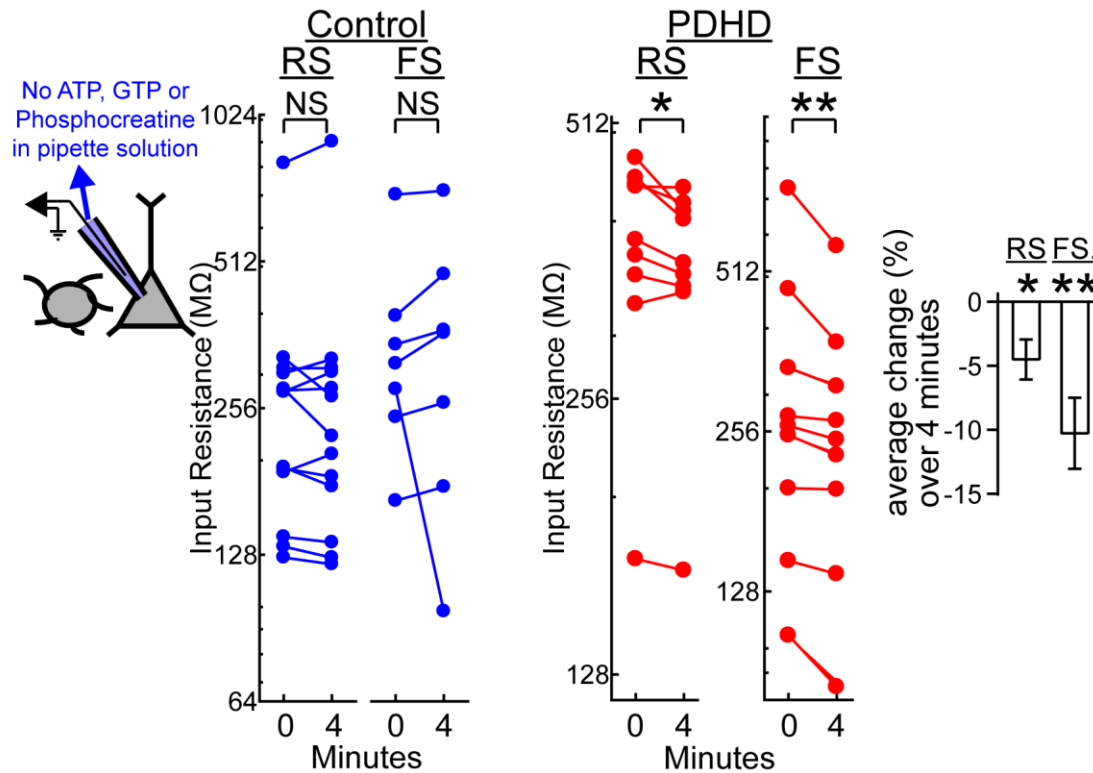


Fig. S12. Neuronal input resistance under energetic substrate deprivation.

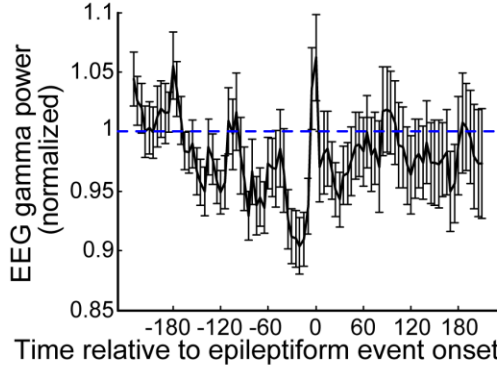
Left: Whole-cell patch-clamp configuration with pipette internal solution devoid of ATP, GTP and phosphocreatine. *Middle and Right:* (i) Input resistance following 4 min dialysis in control neurons with pipette solution lacking energy substrates (regular-spike adapting: n= 13 cells, 11 mice; fast-spike: n= 6 cells, 5 mice) and neurons from PDHD mouse slices (RS: n= 9 cells, 7 mice; FS: n= 9 cells, 8 mice). Each point represents the input resistance of a neuron.

Asterisks in connected dot plots indicate paired *t*-tests. Asterisks in the bar plot indicate a one sample *t*-test, testing if the data mean was significantly different from the value of zero with zero representing no change in input resistance.

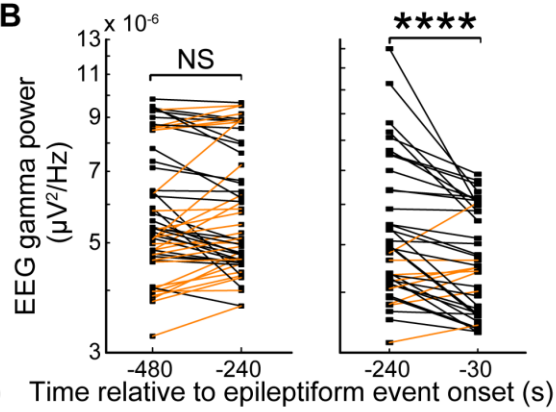
*: $p < 0.05$; **: $p < 0.01$; NS= not significant

Fig. S13

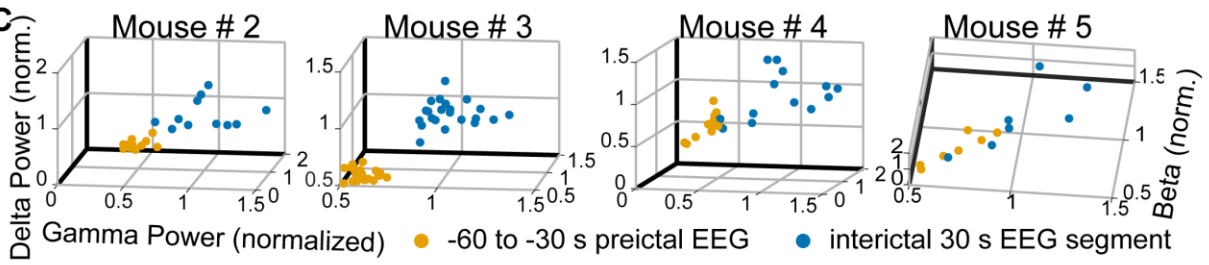
A PDHD Mice



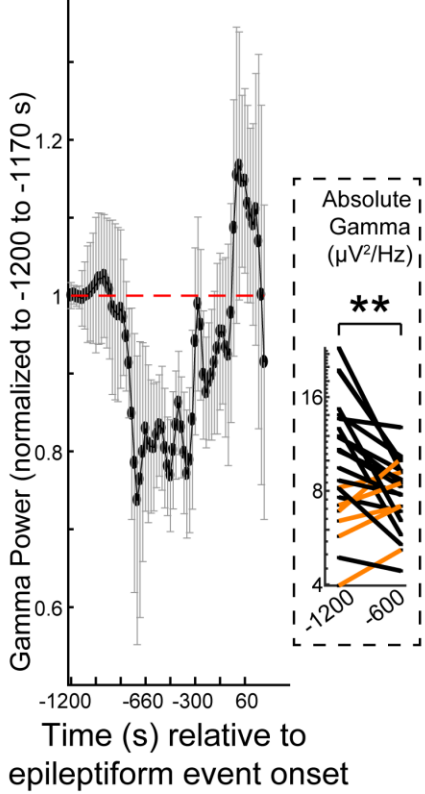
B



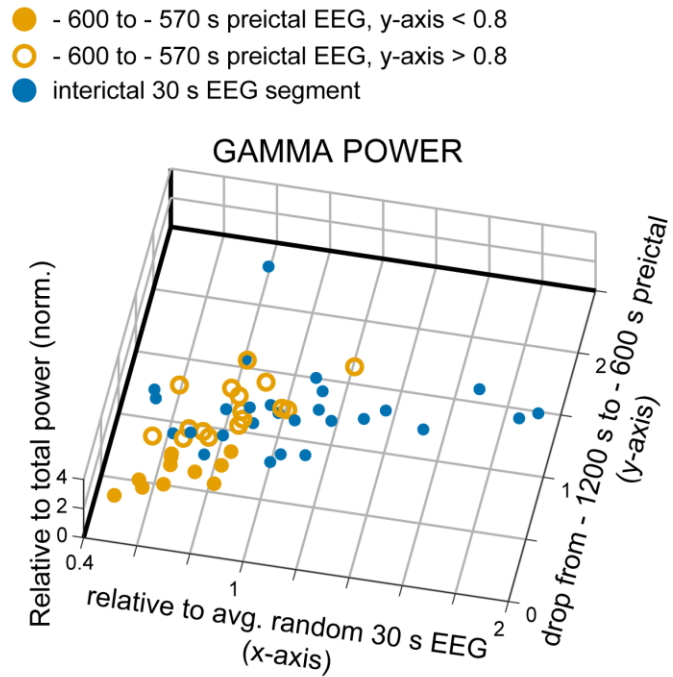
C



D PDHD patient



E PDHD patient



Misclassification rate (10-fold cross-validation) for subset (●) with gamma drop (y-axis) < 0.8 = 0.025

Fig. S13. EEG gamma power in relation to epileptiform events in PDHD.

(A) Gamma oscillation power and epileptiform events in PDHD mice. 39 epileptiform events from 5 mice preceded and followed by at least 4 min of event-free recording were analyzed. The averaged gamma power evolution represented was calculated after normalizing the gamma power of each segment of interest to the power of the same recording during seconds 240 to 120 prior to the epileptiform event. Each data point corresponds to the average gamma power of a 5 s interval, averaged across the 39 epileptiform events analyzed and displayed in temporal relation to event onset (designated as 0 s). Error bars reflect S.E.M.

(B) Evolution of gamma power in relation to epileptiform event onset (occurring at time 0 s) in PDHD mice (n=39 events, 5 mice). Each data point represents the average gamma power of the 30 s that follow the times indicated in the figure (determined from the average power of six 5-second segments). The connecting lines illustrate decreasing (black) or increasing (orange) power.

(C) Preictal and interictal EEG power. Individual PDHD mouse data contrasting the power of preictal EEG segments with the power of randomly-chosen interictal EEG segments.

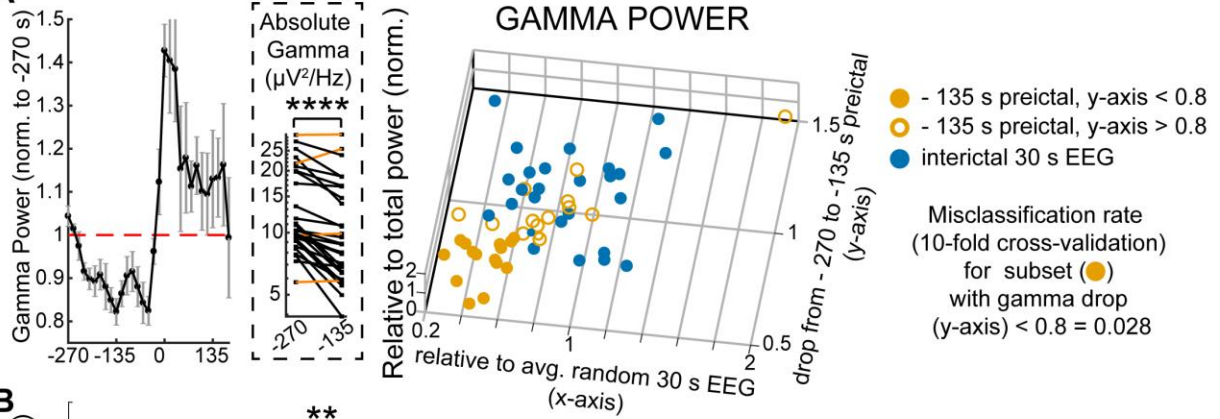
(D) EEG gamma power in a patient with PDHD. 28 epileptiform events preceded by at least 20 event-free minutes were recorded in a single EEG from a PDHD patient. Each data point represents the average and S.E.M of the gamma power of the 10 s that preceded and followed across the 28 events analyzed. Each gamma power value used for averaging was previously normalized to the gamma power of the period from 1200 to 1170 s prior to the related epileptiform event.

(E) Preictal EEG power in a patient with PDHD. Preictal EEG segment gamma power drop (y-axis < 0.8) contrasted with randomly-selected interictal EEG segments of similar duration obtained from the same EEG recording channel. A machine learning protocol was used to examine whether preictal segments could be classified as distinct from interictal segments (quantified using misclassification rate).

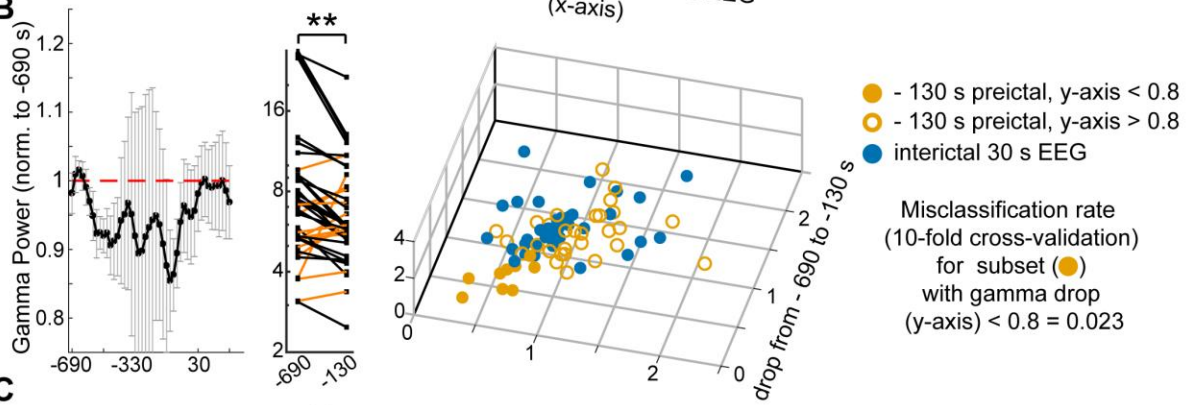
Asterisks indicate paired *t*-tests. **: $p < 0.01$; ****: $p < 0.0001$; NS= not significant

Fig. S14

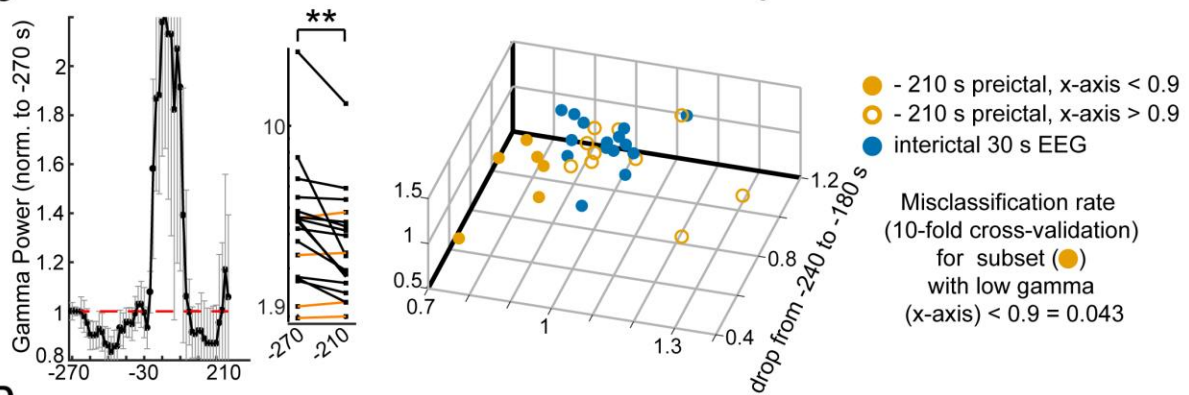
A



B



C



D

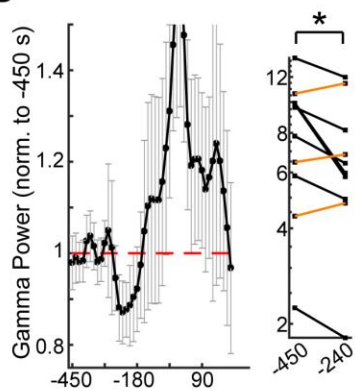


Fig. S14. Gamma power in relation to epileptiform events in additional patients with PDHD.

A-D, left and middle panels. Analysis of all epileptiform events detected in genetically-confirmed PDHD patients. All the events ($n=29, 40, 28$ and 10 events for patients A, B, C and D in Fig. S7, respectively) occurred after uninterrupted event-free EEG segments (which spanned the preceding $270, 690, 270$ and 450 s, respectively) and are represented. Each data point corresponds to the average and S.E.M. of the gamma power of the preceding and following 10 s interval and is averaged across all the events selected for that patient. The gamma power of each event was normalized to the initial 30 s of the same EEG segment. Each point in the middle panel depicts the absolute (raw) gamma power averaged for a 30 s segment beginning at the time noted on the x-axis.

A-C, right panels. Scatter plot of PDHD patients illustrating pre epileptiform-event gamma power in orange (including raw power, power variation and power relative to total EEG power on the x, y and z-axis, respectively) normalized to a random inter-event EEG segment recorded from the same EEG channel. Each point represents the average of a 30 s period beginning at the time indicated. The lower number of events in the right panels relative to the left-middle panels stemmed from the occurrence, in some channels, of fewer event-free EEG segments of appropriate length for normalization. Pre-event EEG segments containing changes in gamma (y-axis < 0.8 for patients in A and B and x-axis < 0.9 for patient in C) are contrasted with interictal events (blue dots). A machine learning protocol examined whether preictal segments could be classified as distinct from interictal segments (quantified using misclassification rate). The patient in (D) demonstrated an insufficient number of events to attempt further analysis.

Values represent mean \pm S.E.M. *: $p < 0.05$; **: $p < 0.01$; ****: $p < 0.0001$. Asterisks indicate paired t -tests.

Fig. S15

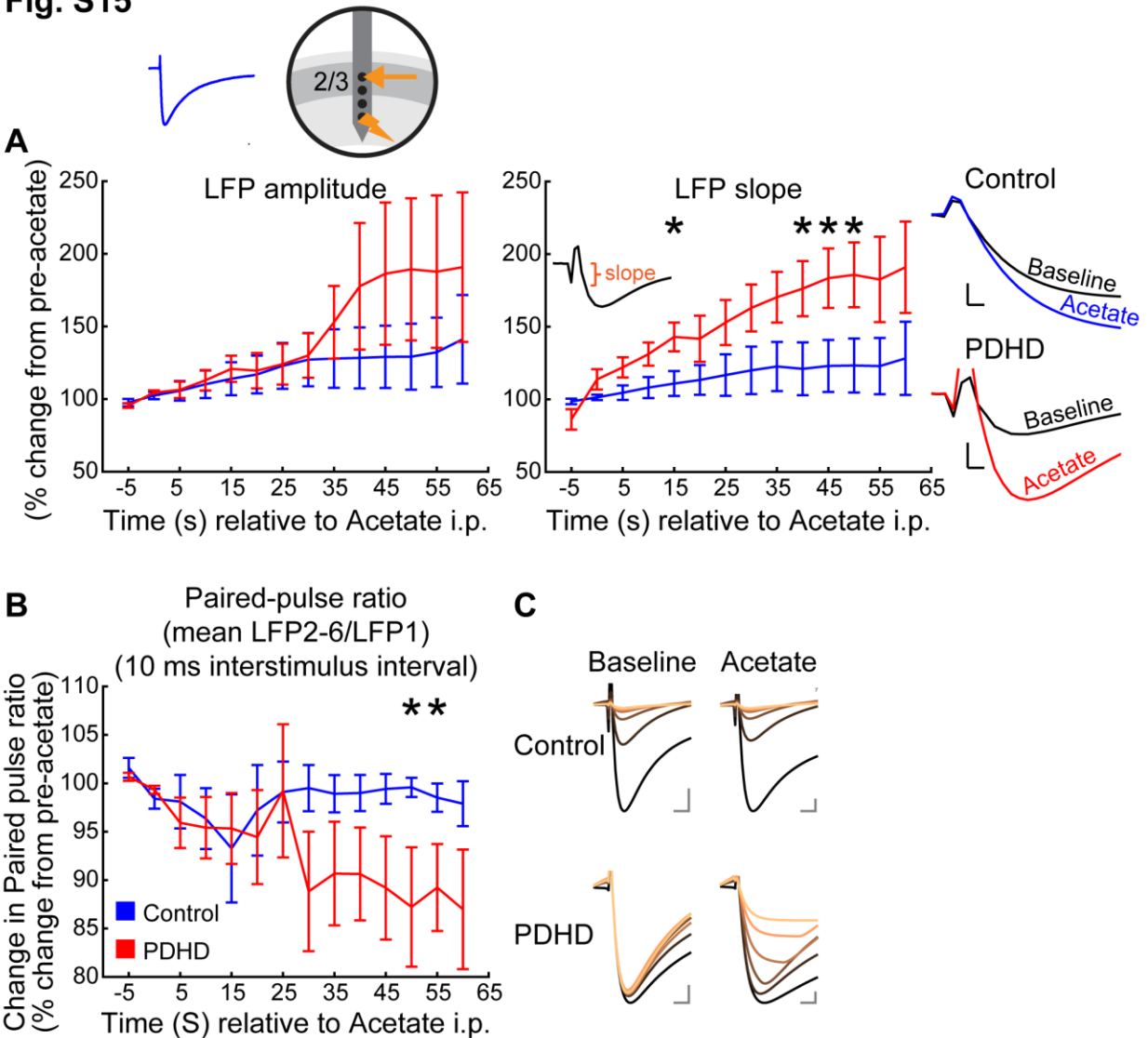


Fig. S15. Acetate modulation of evoked LFPs in vivo.

(A) *Top*: Intracortical stimulus evoking a local field potential (LFP) in the mouse. *Left and middle* - Population of stimulus-evoked LFP amplitude and slope following acetate administration. Each point includes the average of the following 5 min. Inset for LFP slope: first 10-50% of the LFP response used to determine the slope. *Right* - LFP responses of control and PDHD cortex previously to and 45 min following acetate administration. Scale bars: 50 mV, 0.2 ms.

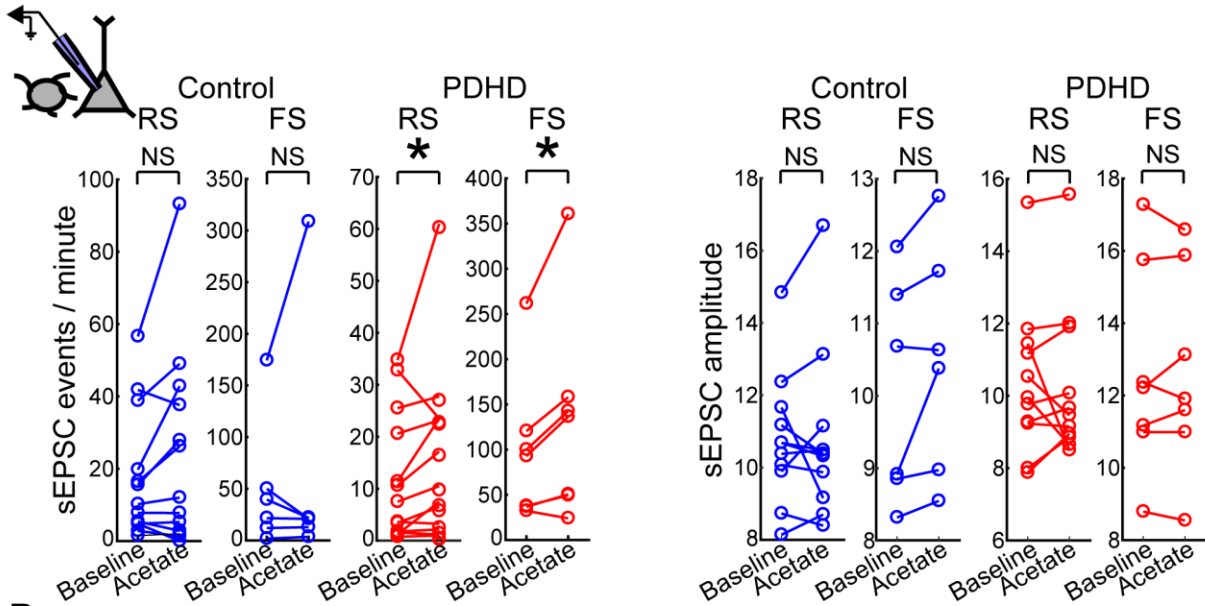
(B) Population average (across all mice) for intracortical stimulus evoked LFP paired-pulse ratios. Each point represents averaged responses obtained in the preceding 5 min. (Control, n= 5; PDHD n =14 mice).

(C) Control mouse recording illustrating robust paired-pulse suppression for a train of 6 stimuli with an inter-stimulus interval of 10 ms (the color tracing of the LFP is progressively lighter with each successive stimulus in a train of 6 stimuli). Scale bars: 50 mV, 1 ms.

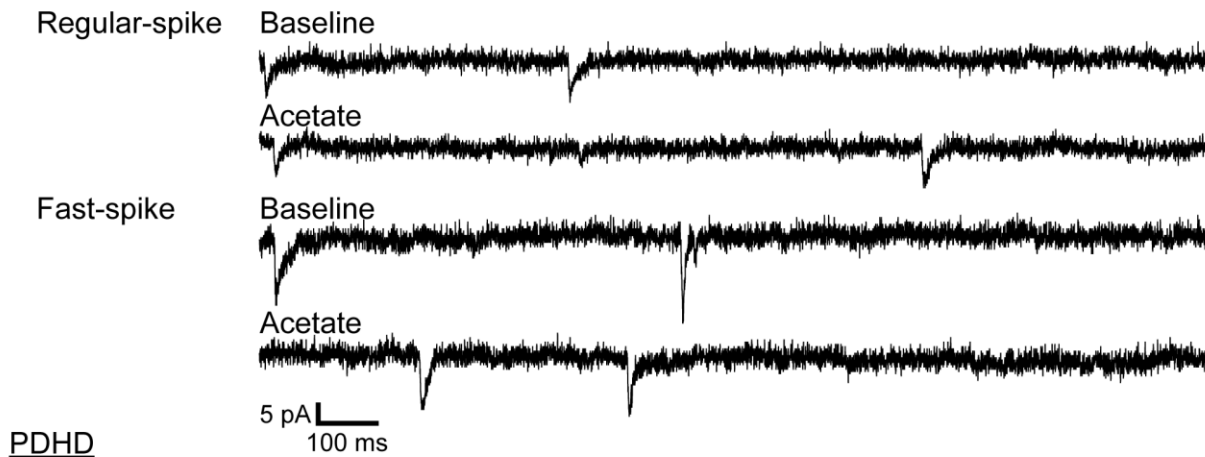
Data represent mean \pm S.E.M. Statistical differences were determined using two-tailed Student's *t* test. *: $p < 0.05$.

Fig. 16

A Spontaneous excitatory post-synaptic currents



B Control



PDHD

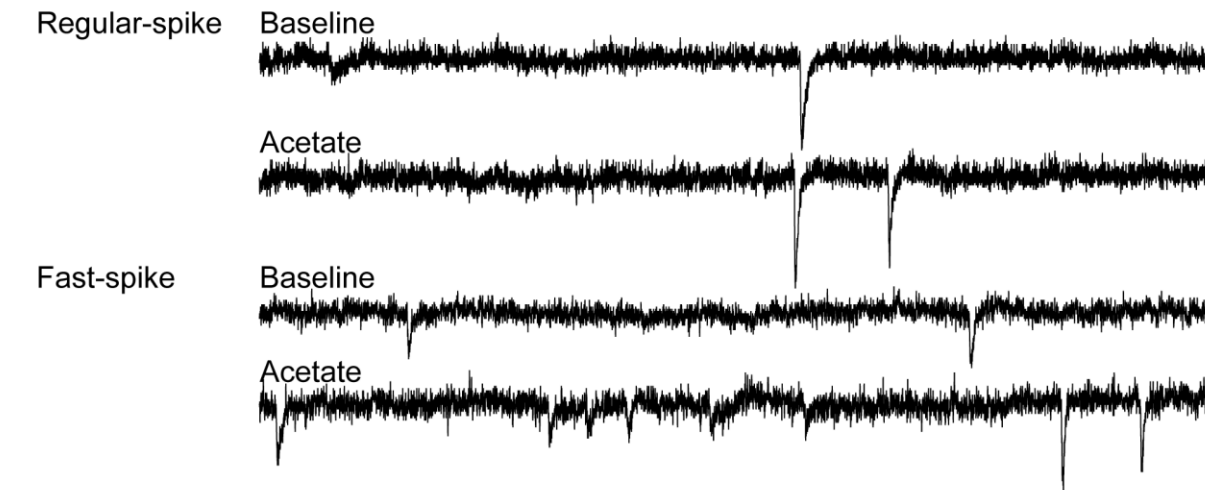


Fig. S16. Acetate modulation of spontaneous excitatory postsynaptic currents.

(A) *Upper left*: Schematic diagram of the whole-cell patch-clamp configuration used in brain slices. *Below and right*: Spontaneous excitatory post-synaptic current frequency and amplitude following acetate administration in PDHD regular-spike adapting (n= 13 cells, 8 mice) and fast-spiking (n= 7 cells, 6 mice) neurons and control (regular-spike adapting, n= 13 cells, 10 mice; fast-spike n= 6 cells, 5 mice) neurons. Asterisks reflect paired *t*-tests.

(B) sEPSC recordings from control and PDHD neurons before and after acetate administration.

Values reflect mean \pm S.E.M. Asterisks indicate paired *t*-tests. *: $p < 0.05$. NS = not significant.

Fig. S17

A Modulation of PDHD input resistance with acetate

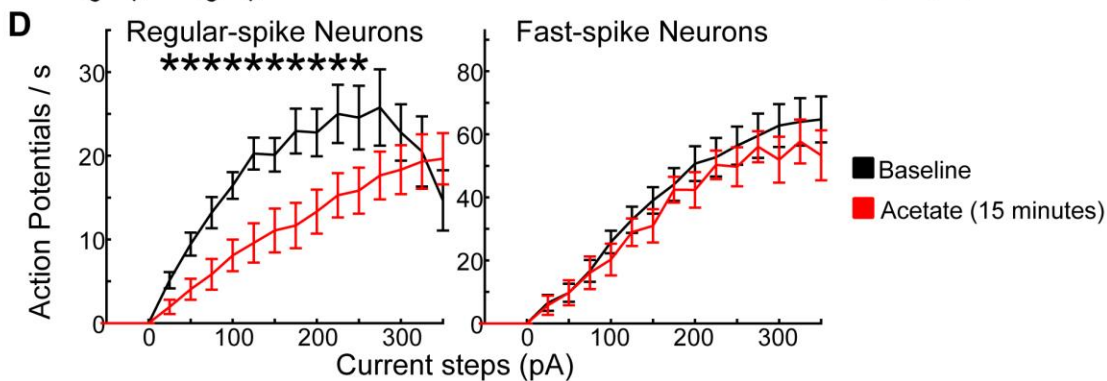
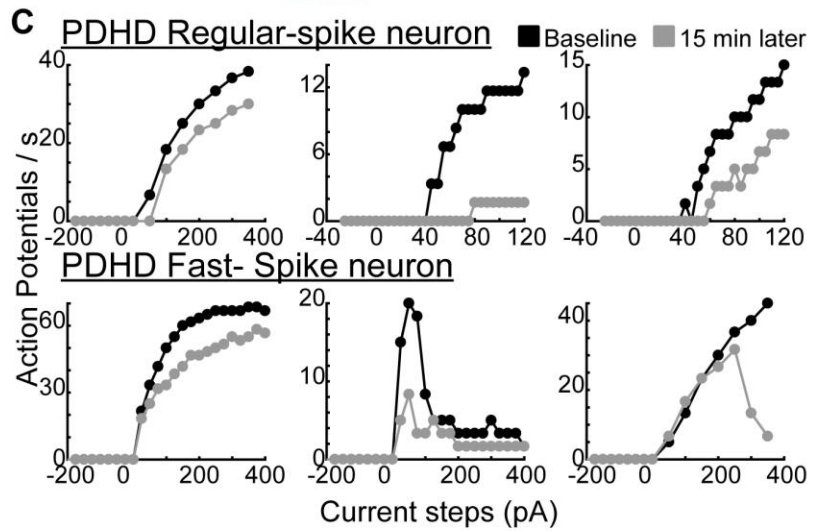
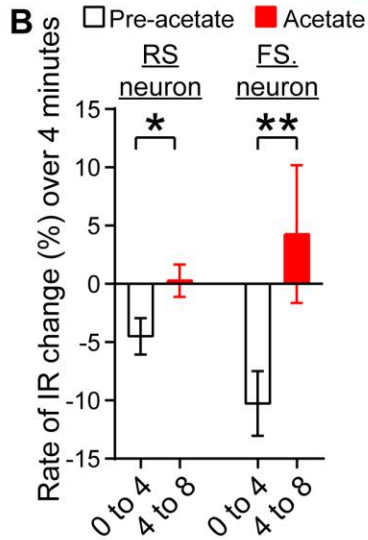
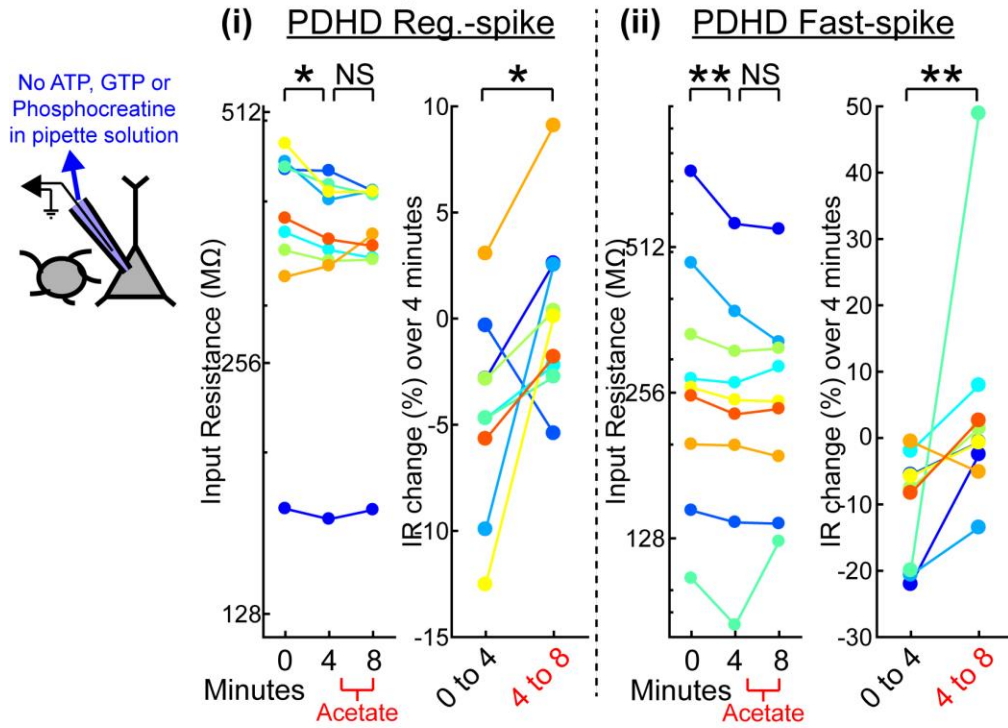


Fig. S17. Modulation of input resistance and firing with acetate.

(A) (i) Left – Effect of acetate applied for 4 min on input resistance of PDHD regular-spike adapting cells with pipette solution devoid of energetic compounds (n= 9 cells, 7 mice). Each neuron is represented in a unique color to follow input resistance changes before and after acetate. Right - Percentage input resistance change over 4 min (the colors match the data on the left). (ii) Fast-spiking PDHD neurons plotted as in (i) (n= 9 cells, 8 mice). Asterisks indicate paired t-tests.

B) Data from (A) represented as population averages..

C) Neuronal firing after prolonged (15 min) dialysis using a pipette solution devoid of ATP, GTP and phosphocreatine.

D) Population average firing before and after 15 min of acetate administration in fast-spiking neurons (n= 12 cells, 10 mice), and regular-spike adapting neurons (n= 15 cells, 9 mice) following 15 min of neuronal dialysis using a pipette solution without ATP, GTP and phosphocreatine.

Values indicate mean \pm S.E.M. Statistical differences were determined using two-tailed

Student's *t* test. *: $p < 0.05$, **: $p < 0.01$, NS = not significant.

Fig. S18.

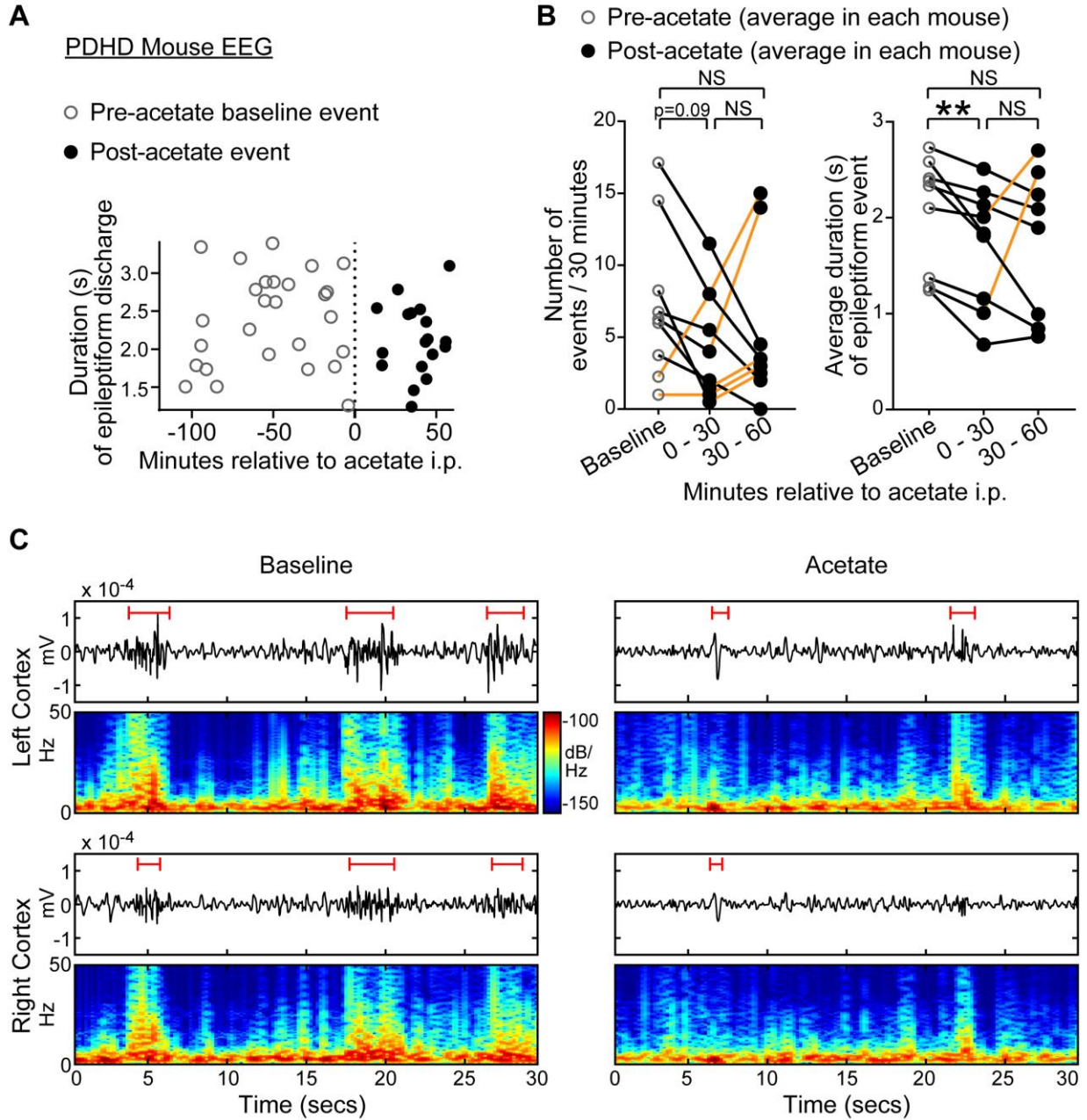


Fig. S18. Acetate modulation of EEG epileptiform events in awake mice.

(A) Time course of epileptiform events recorded by EEG in a PDHD mouse. Each event is represented by an empty or filled circle depending on acetate administration.

(B) Number of epileptiform events and average event duration per mouse (n= 9 mice, calculated for each hemisphere EEG channel, then averaged for both hemispheres for each mouse). Each

mouse is represented by an empty (baseline) or filled (post-acetate) circle. Acetate was injected intraperitoneally following baseline recording for 120 min. Lines connecting decreasing values are black; those between increasing or constant values, orange.

(C) Example EEG traces and spectrograms from a PDHD mouse before (left) and after (right) administration of intraperitoneal acetate. Red lines above traces illustrate durations of epileptiform events.

Statistical differences were determined using paired *t* test. **: $p < 0.01$, NS = not significant.

Fig. S19.

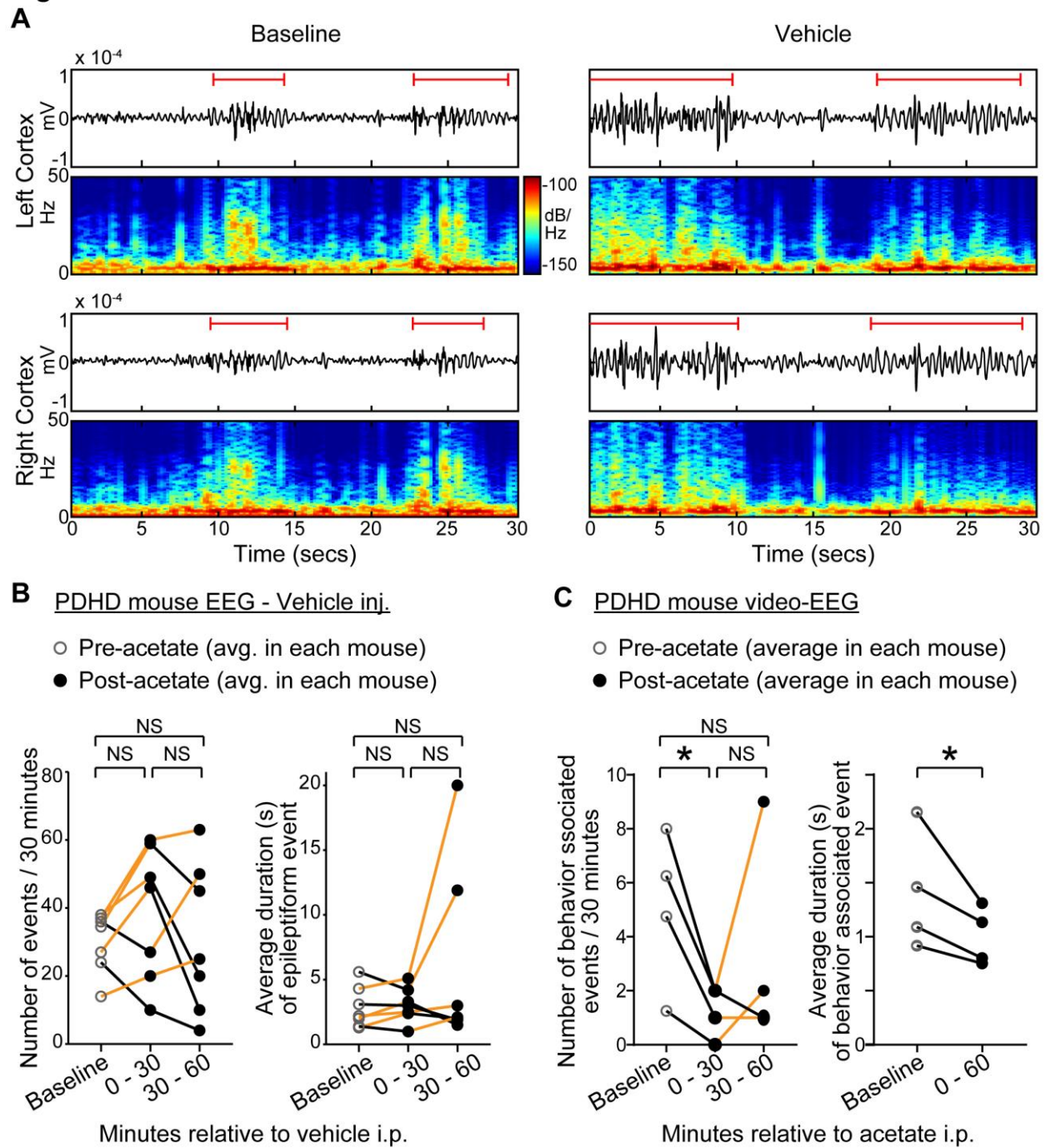


Fig. S19. EEG epileptiform events in awake mice with vehicle injections.

(A) Example EEG traces from a PDHD mouse before (left) and after (right) administration of i.p. vehicle (saline - 0.9% NaCl). Red lines above traces illustrate durations of epileptiform events.

(B) Number of epileptiform events and average event duration per mouse (n= 7 mice, calculated for each hemisphere EEG channel, then averaged for both hemispheres for each mouse) at baseline and after intraperitoneal vehicle (saline – 0.9 % NaCl) injection. Each mouse is represented by an empty (baseline) or filled (post-acetate) circle. The vehicle was injected intraperitoneally after baseline recording for 120 minutes. Lines connecting decreasing values are black; those between increasing or unchanged values are orange. (C) Analysis of impact of acetate on epileptiform events associated with behavioral changes (movement) in 4 PDHD mice. Average event duration was determined for 60 min to include a mouse that exhibited no events within 30 min after acetate. Events were pooled for both channels in each mouse. Lines are colored as in (B).

Values reflect mean \pm S.E.M. Asterisks indicate paired *t*-tests. *: $p < 0.05$; NS = not significant.

Fig. S20

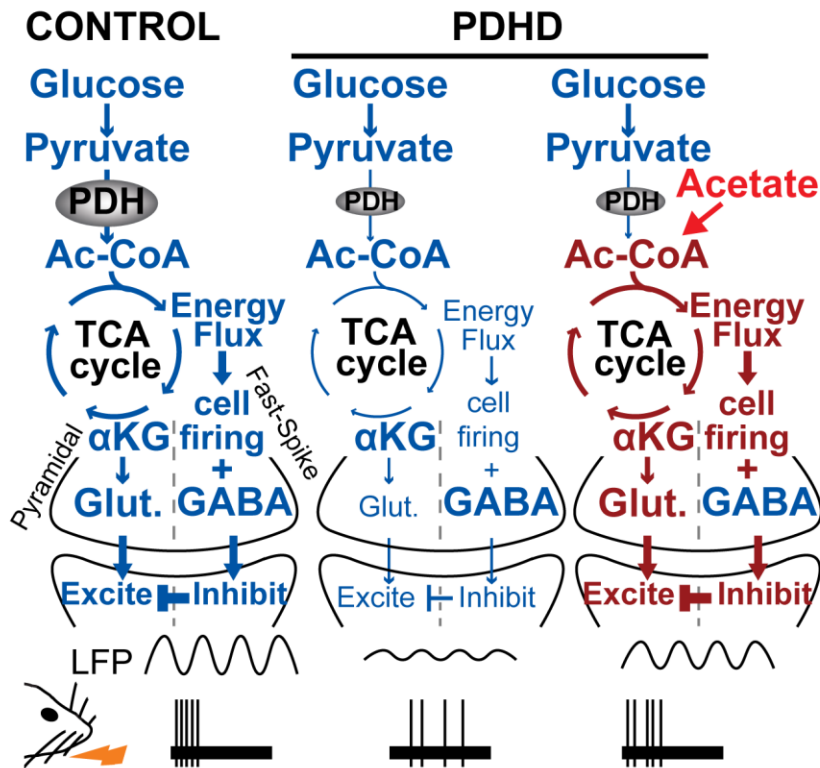


Fig. S20. Representation of glucose oxidation and excitability coupling in relation to PDH activity.

In normal glutamatergic neurons, glucose oxidation generates the neurotransmitter glutamate used for synaptic excitation, whereas in fast-spiking inhibitory neurons energy flux-derived products (for example ATP) maintain cell firing, curtailing excessive excitatory firing. Their concerted action gives rise to robust spontaneous LFP oscillations and time-limited evoked action potentials. In PDHD, deficient glucose oxidation in glutamatergic and GABAergic neurons leads to a reduction in glutamate generation and cell firing, respectively, selectively decreasing glutamate abundance while unrestraining weak—but uninhibited—excitation that

results in prolonged excitatory bursts. Bypassing the PDH enzymatic reaction with acetate enhances glutamate neurotransmission and associated synaptic activation and mitigates inhibitory failure, thus curtailing unchecked excitatory firing and decreasing epileptiform event duration. Oxidative metabolism impacts cerebral cortical excitability by enhancing glutamatergic activation as well as increasing inhibitory neuron excitability to prevent prolonged excitatory firing, thus balancing responsiveness to excitatory input.

Supplementary Table S1

Table S1. Plasma metabolite concentration.

Plasma was collected from the same mice as in Fig. 1E to determine the concentration of glucose, lactate, β -hydroxybutyrate (BHB) and acetoacetate by GC-MS. Acetate was measured in a different mouse group (n= 3) after 5 hr of fasting. Data represent mean \pm S.E.M. *: p< 0.05, unpaired two-sided students *t*-test.

Metabolite (mM)	Control	PDHD
Glucose	7.2 \pm 0.54	5.85 \pm 0.73
Lactate	1.28 \pm 0.31	0.93 \pm 0.35
BHB	1.4 \pm 0.18	1.75 \pm 0.36
Acetoacetate	0.18 \pm 0.03	0.29 \pm 0.04*
Acetate	0.53 \pm 0.02	0.45 \pm 0.09

Supplementary Table S2

Table S2. Isotopomer analysis of [U-¹³C]glucose NMR spectra from cerebral cortex NMR spectra.

Fractional amounts of multiplets of glutamate C4, glutamine C4 and GABA C2 from PDHD (n= 5) and control mice (n= 7) expressed as mean ± S.E.M. The fractional amount was calculated from the area of each individual multiplet divided by the total area of the isotopomer. Blanks denote multiplets that are not labeled from [U-¹³C]glucose for each respective isotopomer. Statistical differences were determined using two-tailed Student's *t* test. *: p ≤ 0.05; **: p ≤ 0.01. S: singlet, Dxx: doublet, Q: quartet, N.D.: not detected (also as in Supplementary Table 3).

¹³ C Multiplets	Glutamate C4		Glutamine C4		GABA C2	
	Control	PDHD	Control	PDHD	Control	PDHD
S	0.055±0.004	0.084±0.006**	0.082±0.009	0.111±0.023	0.031±0.003	0.046±0.002**
D34	0.02±0.001	0.022±0.01	0.025±0.01	0.013±0.009		
D45	0.635±0.007	0.705±0.018**	0.71±0.01	0.79±0.026**		
D23					0.029±0.01	0.013±0.004
D12					0.615±0.013	0.731±0.056*
Q	0.289±0.008	0.187±0.031**	0.208±0.009	0.098±0.035*	0.324±0.13	0.21±0.053*

Supplementary Table S3

Table S3. Isotopomers derived from [1,2-¹³C]acetate and [1,6-¹³C]glucose in cerebral cortex NMR spectra.

Fractional amounts of glutamate C4, glutamine C4 and GABA C2 multiplets obtained from the cortex of PDHD (n= 10) and control mice (n= 10) expressed as mean \pm S.E.M. Statistical differences were determined using two-tailed Student's t test. *: $p \leq 0.05$; **: $p \leq 0.01$.

¹³ C Multiplets	Glutamate C4		Glutamine C4		GABA C2	
	Control	PDHD	Control	PDHD	Control	PDHD
S	0.602 \pm 0.01	0.376 \pm 0.029***	0.45 \pm 0.033	0.201 \pm 0.023***	0.632 \pm 0.012	0.531 \pm 0.022**
D34	0.215 \pm 0.012	0.119 \pm 0.013***	0.111 \pm 0.011	0.034 \pm 0.007***		
D45	0.151 \pm 0.012	0.419 \pm 0.032***	0.393 \pm 0.025	0.653 \pm 0.025***		
D23					0.214 \pm 0.013	0.165 \pm 0.019
D12					0.153 \pm 0.008	0.284 \pm 0.02***
Q	0.031 \pm 0.004	0.086 \pm 0.007***	0.064 \pm 0.007	0.112 \pm 0.009***	0.001 \pm 0.001	0.019 \pm 0.012

Supplementary Table S4

Table S4. Metabolic model analysis of glutamate and glutamine C4 multiplets from [1,6-¹³C]glucose and [1,2-¹³C]acetate cerebral cortex spectra. The values of the isotopomer analysis from glutamate and glutamine C4 in Supplementary Table 3 were incorporated into a numeric model to quantify acetate and glucose oxidative ratio (*I3*). Values denote mean ± S.E.M. Statistical analysis was performed using independent Student's *t*-test assuming equal variances.

CONTROL

Variable	Cortex 1	Cortex 2	Cortex 3	Cortex 4	Cortex 5	Cortex 6	Cortex 7	Cortex 8	Cortex 9	Cortex 10	Mean	S.E.M.
a	0.0815	0.0576	0.0963	0.085	0.0928	0.0918	0.1113	0.0583	0.0702	0.0722	0.0817	0.005453
b	0.5092	0.2192	0.4690	0.5190	0.5609	0.3883	0.5056	0.5113	0.3674	0.4025	0.44524	0.032267
c	0.0564	0.1504	0.0741	0.0558	0.0492	0.0994	0.0691	0.0441	0.0902	0.0799	0.07686	0.009928
d	0.3529	0.5728	0.3606	0.3403	0.2971	0.4206	0.3139	0.3863	0.4723	0.4453	0.39621	0.026446
e	0.2756	0.4029	0.2798	0.2971	0.2446	0.2729	0.3016	0.2344	0.3250	0.2795	0.29134	0.014909
f	0.7244	0.5971	0.7202	0.7029	0.7554	0.7271	0.6984	0.7656	0.6750	0.7205	0.70866	0.014909
g	2.4235	1.2180	1.9526	2.7094	1.5170	1.3702	1.5752	2.5340	2.8875	1.5944	1.97818	0.192623
h	0.2515	0.0009	0.1832	0.3605	0.1399	0.0011	0.0000	0.3486	0.2768	0.0278	0.15903	0.046231
(a+b)/(c+d)	1.4430	0.3827	1.3007	1.5252	1.8879	0.9231	1.6106	1.3237	0.7780	0.9038	1.20787	0.143058

PDHD

Variable	Cortex 1'	Cortex 2'	Cortex 3'	Cortex 4'	Cortex 5'	Cortex 6'	Cortex 7'	Cortex 8'	Cortex 9'	Cortex 10'	Mean	S.E.M.	TTEST
a	0.1373	0.0855	0.1236	0.0962	0.1068	0.1225	0.1284	0.1199	0.1202	0.1573	0.11977	0.006421	0.000266
b	0.6668	0.4913	0.6246	0.7528	0.5637	0.6168	0.7245	0.6724	0.7047	0.6837	0.65013	0.024813	8.63E-05
c	0.0335	0.0627	0.0416	0.0171	0.0525	0.0432	0.0221	0.0314	0.0255	0.0297	0.03593	0.004467	0.001435
d	0.1624	0.3605	0.2101	0.1339	0.2769	0.2175	0.1249	0.1763	0.1496	0.1293	0.19414	0.023866	2.22E-05
e	0.3143	0.0628	0.3503	0.2653	0.2641	0.3093	0.2961	0.2944	0.2992	0.2404	0.26962	0.024933	0.464316
f	0.6857	0.9372	0.6497	0.7347	0.7359	0.6907	0.7039	0.7056	0.7008	0.7596	0.73038	0.024933	0.464316
g	0.8571	0.2815	0.7478	0.4522	1.1978	0.8310	0.1694	0.6256	0.3260	0.4949	0.59833	0.099673	5.41E-06
h	0.0000	0.0000	0.0000	0.0000	0.0535	0.0008	0.0000	0.0000	0.0025	0.0000	0.00568	0.005319	0.004023
(a+b)/(c+d)	4.1047	1.3629	2.9728	5.6209	2.0356	2.8358	5.7991	3.8142	4.7098	5.2859	3.85417	0.483941	5.49E-05

Supplementary Table S5

Table S5. Modified Racine's scale. Modified Racine Scale used to score EEG epileptiform event associated behaviors in mice that underwent video-EEG recording for 2 hr baseline.

Score	Behavioral Stage
1	Sudden behavioral arrest, motionless staring (with orofacial automatism)
2	Head nodding, neck jerks
3	Forelimb clonus with lordotic posture
4	Forelimb clonus, with rearing and/or falling
5	Generalized tonic-clonic activity with loss of postural tone, wild jumping

Supplementary Table S6

Table S6. Key clinical features of patients with PDHD. Clinical features of patients with PDHD whose EEGs were analyzed in the study.

Subject	Age	Gender	Clinical notes
I	2.5 m	M	Severely hypoplastic brain, minimal neurological development beyond neonatal stage, hypotonia, feeding difficulty, chronic and acute respiratory distress, sleep apnea, daily generalized and multifocal seizures
II	5 m	F	Brain cystic lesions, white matter paucity, corpus callosum hypoplasia, minimal neurological development beyond early infancy stage, daily generalized tonic-clonic seizures and staring episodes
III	5 m	F	Moderately hypoplastic brain, white matter paucity, hydrocephalus, moderately abnormal neurological development progressing well below age-expected, weekly generalized tonic-clonic and multifocal seizures
IV	2 y	F	Minimally hypoplastic cerebellum, hypotonia, mild development delay progressing slightly below age expected, sleep apnea, strabismus, exotropia
V	8 y	F	Moderately hypoplastic brain, thalamic necrosis, neurological development stagnation at late childhood, daily tonic and focal seizures

Table S7. Raw data (provided as a separate Excel file).

Movie S1. PDHD mouse video-EEG recording of epileptiform events.

Left: Mouse exhibiting (1) a generalized tonic-clonic seizure and (2) a brief epileptiform event associated with abrupt behavioral (movement) change.

Right: Corresponding EEG (top) and EEG power spectrogram (bottom).